THE STUDY OF RUDDER EFFECTIVENESS AND CONTROL SURFACE REVERSAL OF AN AIRCRAFT HAVING TWIN VERTICAL TAIL

A THESIS SUBMITTED TO
THE GRADUATE SCHOOL OF NATURAL AND APPLIED SCIENCES
OF
MIDDLE EAST TECHNICAL UNIVERSITY

BY

AYBERK YURTSEVER

IN PARTIAL FULFILLMENT OF THE REQUIREMENTS
FOR
THE DEGREE OF MASTER OF SCIENCE
IN
AEROSPACE ENGINEERING

AUGUST 2023

Approval of the thesis:

THE STUDY OF RUDDER EFFECTIVENESS AND CONTROL SURFACE REVERSAL OF AN AIRCRAFT HAVING TWIN VERTICAL TAIL

submitted by **AYBERK YURTSEVER** in partial fulfillment of the requirements for the degree of **Master of Science** i**n Aerospace Engineering, Middle East Technical University** by,

Prof. Dr. Halil Kalıpçılar
Dean, Graduate School of **Natural and Applied Sciences** _____

Prof. Dr. Serkan Özgen
Head of the Department, **Aerospace Engineering** _____

Prof. Dr. Yavuz Yaman
Supervisor, **Aerospace Engineering, METU** _____

Examining Committee Members:

Assoc. Prof. Dr. Ercan Gürses
Aerospace Engineering, METU _____

Prof. Dr. Yavuz Yaman
Aerospace Engineering, METU _____

Assoc. Prof. Dr. Halil Ersin Söken
Aerospace Engineering, METU _____

Prof. Dr. Ender Ciğeroğlu
Mechanical Engineering, METU _____

Prof. Dr. Erdem Acar
Mechanical Engineering, TOBB ETU _____

Date: 25.08.2023

I hereby declare that all information in this document has been obtained and presented in accordance with academic rules and ethical conduct. I also declare that, as required by these rules and conduct, I have fully cited and referenced all material and results that are not original to this work.

Name, Surname: Ayberk Yurtsever

Signature:

ABSTRACT

THE STUDY OF RUDDER EFFECTIVENESS AND CONTROL SURFACE REVERSAL OF AN AIRCRAFT HAVING TWIN VERTICAL TAIL

Yurtsever, Ayberk
Master of Science, Aerospace Engineering
Supervisor: Prof. Dr. Yavuz Yaman

August 2023, 99 pages

Aircraft are inherently flexible, and flexibility is an advantage as a design feature for improved flight performance. Therefore, with the increase in flexibility, the increase in performance should be carefully examined, and flexibility should be controllable. The problem attempted in this study is alleviating the minimization of the yaw effectiveness in designing aircraft with twin vertical tails. The thesis study focuses on creating a reduced-order finite element model for an aircraft with twin vertical tails and proposing design changes based on effectiveness values to address the identified problem. The static aeroelasticity analysis was performed using the MSC.Nastran™ package program as a solver while automating the creation of models with different design parameters using the code indigenously written in Python. The effect of these design modifications is then evaluated within the assumed aircraft flight envelope to show the sensitivity of vertical tail and rudder design parameters that affect rudder yaw effectiveness. Various design changes were proposed to keep the rudders controllable and avoid control surface reversal.

Keywords: Aeroelasticity, Beam – Stick Model, Twin Vertical Tail, Control Surface Reversal, Rudder Yaw Effectiveness

ÖZ

ÇİFT DİKEY KUYRUKLU BİR UÇAĞIN KANATÇIK TERSLİĞİNİN VE DÜMEN ETKİNLİĞİNİN İNCELENMESİ

Yurtsever, Ayberk
Yüksek Lisans, Havacılık ve Uzay Mühendisliği
Tez Yöneticisi: Prof. Dr. Yavuz Yaman

Ağustos 2023, 99 sayfa

Uçaklar yapısı gereği esnektir ve esneklik, daha iyi uçuş performansı için avantaj sağlar. Bu nedenle, esneklik arttıkça performans artışı dikkatle incelenmeli ve esneklik kontrol edilebilir düzeyde olmalıdır. Bu çalışmada ele alınan sorun, çift dikey kuyruklu uçakların tasarımında dümen etkinliğinin azalmasının engellenmesidir. Tez çalışması, çift dikey kuyruklu bir uçak için indirgenmiş bir sonlu eleman modeli oluşturmayı ve etkinlik değerlerine dayalı tasarım değişiklikleri önermeyi hedeflemektedir. Statik aeroelastisite analizi için MSC.Nastran™ paket programı çözücü olarak kullanılmış ve farklı tasarım parametrelerine sahip modellerin otomatik olarak oluşturulması için Python dilinde özgün bir kod kullanılmıştır. Bu tasarım değişikliklerinin etkisi daha sonra, dümen yalpalama etkinliğini etkileyen dikey kuyruk ve dümen tasarım parametrelerinin hassasiyetini göstermek amacıyla varsayılan uçak uçuş zarfı içinde değerlendirilmiştir. Dümenlerin kontrol edilebilirliğini sağlamak ve kanatçık tersliğini önlemek için çeşitli tasarım değişiklikleri önerilmiştir.

Anahtar Kelimeler: Aeroelastisite, Kiriş – Çubuk Modeli, Çift Dikey Kuyruk, Kanatçık Tersliği, Dümen Sapma Etkinliği

To my family…

ACKNOWLEDGMENTS

I would like to express my deepest gratitude to my thesis advisor, Prof. Dr. Yavuz Yaman, for his support, guidance, and valuable insights throughout the thesis study. His dedication to excellence has been truly inspiring, and I consider myself privileged to have had the opportunity to work with him as an engineer in the aerospace industry.

I am also thankful to my thesis committee members, Assoc. Prof. Dr. Ercan Gürses, Assoc. Prof. Dr. Halil Ersin Söken, Prof. Dr. Ender Ciğeroğlu, and Prof. Dr. Erdem Acar for their valuable comments and constructive criticisms that significantly contributed to the quality of the thesis study.

I wish to express my appreciation to Turkish Aerospace for granting the necessary permissions. My gratitude extends to my supervisor, Fatih Mutlu Karadal, for his advice in shaping the thesis topic. I would like to acknowledge my colleagues in the Loads and Aeroelasticity Group, with special recognition for Murat Aydın; his support was vital throughout my thesis studies. Furthermore, I want to offer my special thanks to Betül Keçici for her technical and motivational support during my thesis study.

Finally, I am deeply grateful to my parents, Aygül Yurtsever and Yüksel Yurtsever, and my brother, Arda Yurtsever, for their endless support throughout my education.

This thesis would not have been possible without these individuals' and organizations' collective support and contributions. Thank you all for being part of this journey.

TABLE OF CONTENTS

LIST OF TABLES

TABLES

LIST OF FIGURES

FIGURES

LIST OF ABBREVIATIONS

ABBREVIATIONS

AIC: Aerodynamic Influence Coefficient

CFD: Computational Fluid Dynamics

DLM: Doublet-Lattice Method

DOE: Design of Experiments

ESDU: Engineering Sciences Data Unit

FAR: Federal Aviation Regulations

FE: Finite Element

FLDS: MSC Patran FlightLoads™

GUI: Graphical User Interface

IPS: Infinite Plate Spline

LEF: Leading Edge Flap

NACA: National Advisory Committee for Aeronautics

NASA: National Aeronautics and Space Administration

OML: Outer Mold Line

TEF: Trailing Edge Flap

VT: Vertical Tail

LIST OF SYMBOLS

SYMBOLS

b	Wing span
c	Chord length
e	Distance to elastic axis
L	Lift
l	Roll maneuver
m	Pitch maneuver
n	Yaw maneuver
p	Roll rate
q	Pitch rate
r	Yaw rate
S	Reference wing area
$\bar{q}$	Dynamic pressure of the air
α	Angle of attack
β	Sideslip angle
δ	Control surface deflection angle
θ	Pitch angle
k_t	Rotational stiffness of the support
M_{ac}	Pitching-moment about the aerodynamic center
C_L	Lift coefficient
$C_{M_{ac}}$	Aerodynamic moment coefficient
U	Freestream airspeed
ρ_∞	Freestream air density
C_{M_0}	Pitching-moment coefficient due to asymmetric airfoil
C_{M_δ}	Pitching-moment coefficient due to control surface deflection
C_{L_α}	Lift curve slope of the airfoil

q_D	Dynamic pressure for divergence
q_R	Dynamic pressure for control surface reversal
$[D]$	Rigid body mode matrix
$[K_{aa}]$	Structural stiffness matrix
$[M_{aa}]$	Structural mass matrix
$[Q_{aa}]$	Aerodynamic influence coefficient (AIC) matrix
$[Q_{ax}]$	AIC matrix due to unit deflections of the aerodynamic extra points
$\{p_a\}$	Applied loads vector
$\{u_x\}$	Aerodynamic extra points vector as input
$\{u_a\}$	Structural analysis set points vector
$\{\ddot{u}_a\}$	Structural accelerations vector
$\dot{p}$	Roll rotational acceleration
$\dot{q}$	Pitch rotational acceleration
$\dot{r}$	Yaw rotational acceleration
$\ddot{u}_2$	Translational acceleration for y-axis
$\ddot{u}_3$	Translational acceleration for z-axis
δ_{ail}	Aileron deflection angle
δ_{ht}	Horizontal tail deflection angle
δ_{rud}	Rudder deflection angle
b_{VT}	Height of the vertical tail
S_{VT}	Reference wing area for the vertical tail
AR_{VT}	Aspect ratio for the vertical tail
λ	Taper ratio
η	Effectiveness value
C_r	Chord length at the root of the vertical tail
C_t	Chord length at the tip of the vertical tail

CHAPTER 1

INTRODUCTION

1.1 Background of the Study

Aircraft are inherently flexible, and flexibility is an advantage as a design feature for improved flight performance [1]. However, instability due to flexibility can cause dangerous damage to aircraft. Therefore, with the increase in flexibility, the increase in performance should be carefully examined, and flexibility should be at a controllable level. A flexible aircraft must withstand the combined effects of aerodynamic, elastic, and inertial forces within its flight envelope.

The problem attempted in this study is the alleviation of the minimization of the yaw effectiveness in the design of aircraft having twin vertical tails. This is a control surfaces effectiveness problem encountered in static aeroelasticity. The aerodynamic loads resulting from control surface deflections cause wing deformation and loss of efficacy for the control surface. It appears under a static balance between the elastic restoring moments and the aerodynamic moments on the system [2]. Control surface effectiveness indicates the ability of a particular control surface to generate a rolling moment, and control surface reversal occurs when effectiveness is equal to zero [3]. Control surface reversal is a frequently encountered aeroelasticity problem examined during aircraft design development.

Concerning static aeroelastic applications, most of the studies known are focused on improving the design of aircraft wings. However, empennage surfaces such as horizontal tails and vertical tails should also have been investigated in detail to meet the two requirements: sufficient stability and maneuverability for the longitudinal and directional motion of the aircraft. Vertical tail plays a crucial role

in overall aircraft's directional stability and maneuver performance. In the case of vertical tails, the aeroelastic effectiveness of the side force and the rudder yawing moment are usually reduced by the flexibility of the structure [4]. The vertical tail structure has to be strong enough to handle all the forces during different maneuvers. Design solutions that will prevent the problem of low effectiveness might cause a weight increase for the structure, which is disagreeable due to the possible backward shift of the center of gravity. Therefore, it is much more important today to know the aeroelastic properties of the aircraft as early as possible in the design process. A solution for weight increment, without any structural problems, would be welcomed in the design stage, provided that it will also lead to better performance.

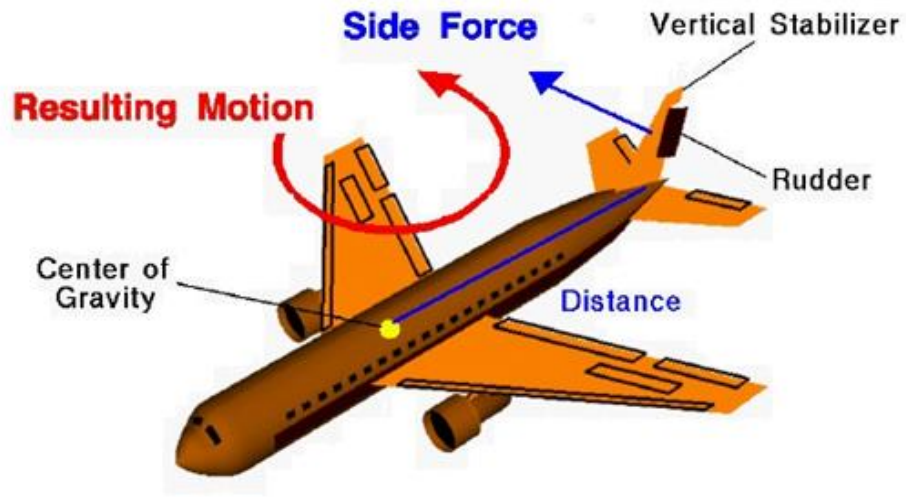

Figure 1.1 Drawing Representing Vertical Tail (Stabilizer) and Rudder [5]

The vertical tail, or stabilizer, is a crucial component of an aircraft's aerodynamic design. It is at the aircraft's rear, extending vertically from the fuselage. Its primary purpose is to ensure the aircraft's stability and control during flight, particularly for its yaw axis. This function involves preventing uncontrolled yawing or sideslipping, thus maintaining the aircraft on a straight, steady path through the air. Factors such as crosswinds or variations in engine thrust during flight can induce

side forces that may lead to yaw or deviations from the intended flight path. In order to counteract these forces and maintain stable flight, the vertical tail generates a side force at a specific distance from the aircraft's center of gravity. When multiplied by the distance, this side force results in a yawing moment, as shown in Figure 1.1, stabilizing the aircraft and enabling it to maintain a controlled trajectory.

Simultaneously, the rudder, a movable control surface attached to the trailing edge of the vertical tail, plays a critical role in aircraft control. Pilots operate the rudder to induce yawing motion and precisely control the aircraft's heading and direction. Pilots can initiate turns and maintain a desired flight path by deflecting the rudder left or right, making it an for achieving precise control. Eventually, the rudder controls the yaw, facilitating precise control to maintain stable flight.

The weight is an important design parameter in aircraft designs today. When the airplane gets heavier, the vertical tail requires being more extensive and taller for directional stability. However, structural weight increase penalty and hangar requirements are not satisfied in that scenario. Moving the vertical tailback for a more extended moment arm is a solution, but loads increase when it is moved back. One large tail produces more shear force at the root, but two smaller tails mean less force at the vertical stabilizer root. Twin tails are shorter than one big tail, and vertical height is a consideration in modern aircraft. Optimal design of vertical tails not only results in a weight reduction but also reduces aerodynamic drag, radar signature, and dynamic loads from buffeting. For modern aircraft, the ability to fly and maneuver at high angles of attack gives tactical advantages. Maneuverability at very high angles of attack is achieved through the placement of twin vertical tails. High angles of attack cause the airflow to be disturbed by the fuselage or wings unpredictably; therefore, a single vertical tail is not fed sufficiently by the uniform flow. Furthermore, twin tails create less of a radar cross-section and allow the tails to be angled to deflect radar signals away from airborne radar sources. Twin tails are seen on most modern aircraft because of these reasons.

Figure 1.2. Example of an Aircraft with Twin Vertical Tail [6]

Twin vertical tails can be placed at an angle for design purposes. Usually, pitching is done by horizontal tail surfaces. However, slanted vertical tails can aid in the pitching motion. The pitching rotates the aircraft on takeoff and makes it maneuverable at a high angle of attack in air combat. When slanted vertical tails move toe in, they can divert the air to help pitch the airplane up or to be used as airbrakes if necessary. Thanks to that, slanted vertical tails can work together with horizontal tail surfaces for added pitch momentum. In some aircraft where the tails are significantly slanted, they can serve as vertical and horizontal tails.

1.2 Introduction to Aeroelasticity

Aeroelasticity focuses on the aerodynamic, elastic, and inertial forces that impact aircraft structures. This field of study is interested in the interaction between the deformation of an elastic structure in airflow and the aerodynamic force resulting from this deformation. The interdisciplinary nature and relations of the forces mentioned above are demonstrated in Figure 1.3 by Professor A.R. Collar with the aeroelastic triangle [7]. Classical aerodynamic theories estimate the forces acting

on a body of a particular shape. Furthermore, elasticity calculates the shape of an elastic body under a given load. Likewise, dynamics provide the effects of inertial forces [8]. If the aircraft structures were fully rigid, there would be no aeroelastic problems. Modern aircraft structures are flexible, and this flexibility is primarily responsible for various types of aeroelastic phenomena [9]. Structural flexibility may not be a problem, but structural deformations can cause additional aerodynamic forces. These additional aerodynamic forces can produce additional structural deformations that will cause even greater aerodynamic forces. Such interactions may raise and destroy the structure. Aeroelasticity is divided into two main categories as static aeroelasticity and dynamic aeroelasticity.

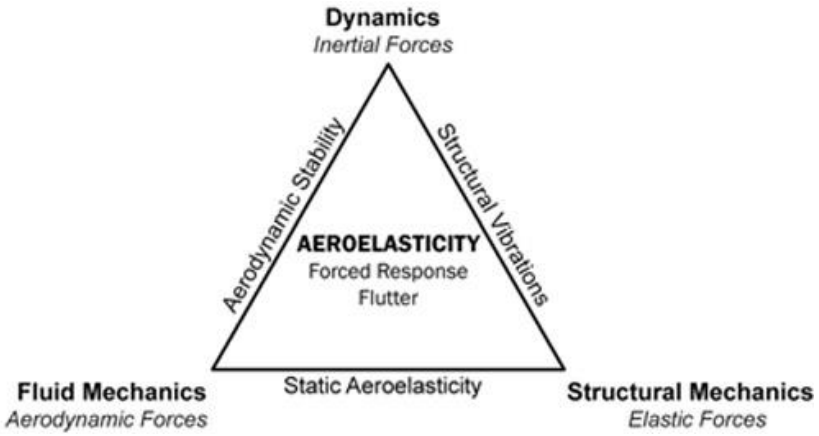

Figure 1.3. Collar's Aeroelastic Triangle [10]

Static aeroelasticity deals with the interplay between aerodynamic and elastic forces. Its primary areas of focus contain the distribution of loads on the flexible wing, phenomena such as divergence and control surface effectiveness, as well as control reversal and aeroelastic impacts on static stability. Furthermore, static aeroelasticity notably influences the static stability, control attributes, and trim performance of aircraft. Static aeroelasticity primarily focuses on the deformation of aircraft structures under aerodynamic loads and how these deformations affect the aircraft's performance. It is concerned with understanding how the structure

responds to these loads while assuming that the aircraft remains steady, not considering dynamic effects like oscillations or maneuvers. In static aeroelasticity, stability, and control effects are typically not the primary focus. Instead, the main concern is ensuring that the aircraft structure remains within its deformation limits, preventing issues like divergence, which is a phenomenon of static aeroelasticity. While the aircraft structure's deformation may influence stability and control characteristics, these effects are often secondary and typically addressed separately in detail in flight mechanics and aircraft dynamics. While static aeroelasticity may indirectly impact stability and control by affecting the aircraft's structural integrity, the detailed analysis of these effects falls within the domain of flight mechanics, which considers the dynamic response of the aircraft to various inputs and disturbances and, hence, to dynamic aeroelasticity. However, there is an indirect connection, and this connection arises from the redistribution of loads across the flexible wing, which directly impacts the aircraft's overall behavior in flight. The changes in wing shape and load distribution induced by aeroelastic effects directly affect the aircraft's flight mechanics. For instance, control surface effectiveness and reversal directly impact the aircraft's ability to maintain a stable flight and respond to pilot commands.

Load distribution is the impact of elastic deformations of the structure on the aerodynamic pressure distribution over the structure. The elastic wing may experience washout, resulting in the loss of its performance. *Divergence* is instability when the elastic moments within the wing structure are exceeded by the aerodynamic moments. The most common type is the wing torsional divergence. The torsional stiffness displays a vital role in the wing divergence phenomenon. The efficiency of the aircraft's control surfaces can be impacted by structural deformations, known as *control surface effectiveness*. In concisely, aeroelastic interactions affect the controllability of the aircraft. Control effectiveness tends to decrease as speed increases until a specific point, known as reversal speed, is reached. At this point, the aircraft will not respond to control surface inputs and, in

some cases, may even move in the opposite direction of the intended movement; this phenomenon is called the reversal of control. *Control surface reversal* happens when the control surfaces twist the wing, causing the aircraft's maneuverability to change direction above a certain speed. In some cases, this can lead to inadequate performance and even move in the opposite direction. *Aeroelastic effects on stability* refer to the influence of elastic deformations of the structure on dynamic and static airplane stability [9].

Dynamic aeroelasticity considers the interaction of inertial, aerodynamic, and elastic forces on an elastic structure in motion. As a result, it considers the unsteady aerodynamic effects that occur. The field is focused on flutter, buffeting, and how structures respond to dynamic loads. *Flutter* refers to an unstable self-excited oscillation of a structure in airflow. Stable oscillations occur when an initial disturbance is introduced to the system at speed below the flutter speed. At the flutter speed, the oscillation amplitude remains constant. However, in the speed exceeds the flutter speed, the airflow negatively impacts the structure, causing the oscillations to increase in amplitude and diverge. Flutter is a phenomenon that can occur in different forms, including wing flutter, control surface flutter, panel flutter, and blade flutter. Wing flutter can be divided into classical bending - torsion flutter and stall or blade flutter, which can occur on wings at a high angle of attack or in rotating blades, like those found in rotorcraft and engines. Control surface flutter, also known as control surface buzz, is typical in transonic regions and may not be catastrophic; however, it is still undesirable. Panel flutter is a major stability issue for aircraft with large panels, and it happens on the surfaces of structures in transonic and supersonic flow regimes. *Buffeting* refers to transient vibrations of aircraft components, mainly the vertical tails, caused by aerodynamic impulses from other aircraft components. *Dynamic response* refers to the structure's transient response to sudden loads such as gusts, landing forces, gun reactions, rapid maneuvers, moving shock waves, or other dynamic loads [9].

1.3 Scope of the Thesis

The evaluation of the aeroelastic effects in the early stages of the design prevents irreversible faulty design. Flexibility effects should be included in the design activities as early as possible. This study aims to create a reduced order finite element model of an aircraft having twin vertical tail and intends to overcome some static aeroelastic problems by calculating and presenting the four fundamental effectiveness values such as aileron roll effectiveness, horizontal tail roll effectiveness, horizontal tail pitch effectiveness, and rudder yaw effectiveness. Finding a three-dimensional generic finite element (FE) model of twin tail aircraft is not easy in the open-source literature. For this reason, it is aimed to automate the production of models with different design parameters with the code indigenously written in Python. The thesis study can be divided into three parts. In the first part, the developed tool will help to create the reduced order model. A reduced order model then allows for aeroelastic effects to be integrated into the early design phases.

The second part of the study analyzes the aircraft in the assumed flight envelope after the completion of the modeling part by using the MSC Patran FlightLoads™ (FLDS) package program for the aerodynamic model and the developed Python code for the structural model. MSC.Nastran™ package program (SOL144 – Static Aeroelasticity Module) was used as a solver for the static aeroelasticity analysis. This solver uses two-dimensional aerodynamic panels based on the Doublet-Lattice Method (DLM) for subsonic speeds and the ZONA51 panel method for supersonic speeds. Since the control surface effectiveness is the ratio of the flexible and rigid aerodynamic stability derivative control coefficients, aerodynamic modeling should be done as accurately as possible. The effectiveness values were determined using Equation 1.1, which relates the change in stability control derivative coefficients to the deflection of the control surface for the specific maneuver being studied (roll (l), pitch (m), and yaw (n)) [3]. This equation calculates the control surface's

effectiveness by considering the ratio between the flexible and rigid wings. Analyzing the resulting effectiveness values shows the change in the control surface's performance due to flexibility.

$$\eta = \frac{\left(\frac{\partial C_{l,m,n}}{\partial \delta_{control\ surface}}\right)_{flexible}}{\left(\frac{\partial C_{l,m,n}}{\partial \delta_{control\ surface}}\right)_{rigid}} \tag{1.1}$$

Aerodynamic effectiveness values generally decrease due to the flexibility of the structure when side force and rudder yaw moment are applied to the vertical tails [4]. Since as compared to other effectiveness values, the yaw effectiveness is expected to be lowest among the other, therefore, the yaw effectiveness is expected to be critical for an aircraft with a twin vertical tail. In aircraft with twin vertical tails, such as the F-18, F-22, and F-35, the yaw moment of the tails becomes less than the designed due to flexibility of the structural elements.

As indicated above, the probable insufficient yaw effectiveness is a big concern in the design of aircraft with twin vertical tails. The negative effects of this inadequate rudder yaw effectiveness condition of twin vertical aircraft will be tried to overcome by proposing design modifications to the vertical tail and rudder design parameters in order to keep the rudders controllable and avoid control surface reversal of vertical tails. In the final part of this thesis, these design changes' impact will be evaluated and presented in the aircraft's assumed flight envelope in order to determine the sensitivity of vertical tail and rudder design parameters that affect rudder yaw effectiveness.

1.4 Content of the Thesis

The first chapter serves as an introduction, providing background information on the topic, an overview of the field of aeroelasticity, the scope of the research, and an outline of the remaining chapters in the thesis.

The second chapter reviews previous literature on control surface effectiveness and control surface reversal of static aeroelasticity.

The third chapter describes the theory behind the control surface effectiveness and control surface reversal of static aeroelastic analyses and details of the MSC.Nastran™ procedure for the type of the analysis used in this thesis.

The fourth chapter explains the finite element modeling of the aircraft's reduced one-dimensional (1D) structural beam-stick model, the two-dimensional (2D) aerodynamic modeling, and the link between these models using spline relation.

The fifth chapter looks at the impact of different design parameters on the control surface effectiveness analyses for the twin vertical tail aircraft on rudder yaw effectiveness, such as torsional stiffness, trailing edge sweep angle, rudder-vertical tail chord ratio, actuator stiffness of the rudder, aspect ratio, taper ratio, and overhang distance, on the considered effectiveness values.

Finally, the sixth chapter presents the general conclusions of the study, as well as suggestions for future research.

CHAPTER 2

LITERATURE REVIEW

The first control surface reversal problem occurred with the Bristol Bagshot, a twin-engine, high-aspect-ratio English aircraft in 1927. As velocity increased, the aileron's effectiveness dropped to zero and became negative. Roxbee Cox and A.G. Pugsley were able to analyze the incident effectively and established design guidelines to prevent it in the early 1930s. While aileron reversal is not a typical failure mode that leads to catastrophic failure, it can be hazardous and is crucial in design considerations [9].

Pugsley [11] summarized the pioneer works on loss and reversal of aileron control. The author aims to use current research on that time about aeroelastic instabilities to provide general design insights and to explain these findings concerning past and present problems. It begins by identifying the primary stability and associated issues, noting the similarities between wings and tailplanes. The paper then discusses these problems, specifically in the context of wings and ailerons. The document discusses alternatives to the traditional solution of increased stiffness.

Broadbent and Mansfield [12] developed a method for determining the speed at which control surface reversal occurs on a swept wing, emphasizing wing sweepback. The procedure is based on strip and semi-rigid theories. The effect of various parameters, such as the degree of sweep, wing torsional and flexural stiffness, wing shape, and aileron shape, are investigated. Graphs are provided that allow for easy estimation of reversal speed by interpolation for a given wing based on variations of these parameters. The results are obtained using simplified models of wing deformation.

Molyneux and Broadbent [13] discussed the theoretical possibility of control reversal due to wing deformation that occurs when a partial-span flap and inset aileron are used. The semi-rigid method is used to investigate this phenomenon for a specific aircraft. The results show that the calculated reversal speed is lower than in the traditional wing-aileron case. The study also looks at how the reversal speed changes with variations in the degree of constraint on the wing and flap, and it concludes that increasing the stiffness at the root of the flap is the most effective way to raise the reversal speed in that case.

The paper by Goland [14] used experimental data to investigate the aerodynamic characteristics of wings and ailerons during the occurrence of aileron reversal. The study includes wind tunnel testing on both a straight wing and a 45-degree sweptback wing at different Mach numbers (0.6, 0.7, 0.8, and 0.85). The outcomes of the wind tunnel tests are illustrated in graphical form and compared to the theoretical and empirical aerodynamic characteristics commonly used in reversal calculations.

Hedgepeth and Ken [15] described a method for analyzing the aeroelastic behavior of a rectangular wing mounted on a cylindrical body at supersonic speeds. The method uses linearized supersonic lifting-surface theory and structural influence coefficients to formulate a numerical solution that incorporates matrices to calculate the rolling effectiveness and aileron-reversal speed. The results obtained from this method for an example configuration are compared to results obtained from simplified analysis methods. The study also examines how the rolling effectiveness varies with the Mach number for two different constant-altitude flights.

The article of Horton [16] is designed to serve two purposes: first, it provides a way to estimate the critical reversal speed of a wing quickly, and second, it explains why approximations can be used for the general formula for determining the reversal coefficient (K) when the aileron chord and wing chord have a linear taper at least over the aileron portion. The article illustrates the relationship

between the aileron-wing chord ratio and the reversal speed. Overall, the paper aims to provide a simple and efficient way to estimate a wing's critical reversal speed and provide insight into why certain approximations can be used in the calculation.

Pearson and Aiken [17] represented a set of charts to determine the wing torsional stiffness required to achieve a certain level of rolling effectiveness. These charts can also be used to quickly calculate the aileron reversal speed and the change in rolling effectiveness with airspeed. The charts apply to linear taper and elliptical wings made of tubular-shell construction and have different aspect ratios. The charts also consider the effect of the aileron span and location on the wing. The derivation of the charts includes the consideration of induced lift effects. Overall, the charts provide an efficient way to quickly estimate the required wing torsional stiffness, aileron reversal speed, and the variation of rolling effectiveness with airspeed for various wings and aileron configurations.

Fischel et al. [18] described a low-speed wind tunnel test conducted to evaluate the lateral control characteristics of a group of untapered, low-aspect-ratio wings. The test specifically looked at sealed flap ailerons of different spans and locations on wings with aspect ratios of 1.13, 2.13, 4.13, and 6.13. Additionally, various projections of 0.60 - semi span retractable ailerons were analyzed on unswept wings with aspect ratios of 1.13, 2.13, and 4.13, as well as on a 45-degree sweptback wing. The paper concludes by stating that design charts are based on the experimental results, which can be used to estimate the effectiveness of flap ailerons on low-aspect-ratio, untapered, and unswept wings.

Andersen, Kolonay, and Eastep [19] conducted a research investigation into the prediction of control-surface reversal during transonic flight. Their approach involved utilizing both linear and nonlinear analyses of the structural and aeroelastic aspects to explore the impact of flow nonlinearities on this aeroelastic phenomenon. This method was employed on two types of wings: a primary rectangular wing and a typical fighter-type wing. Transonic small disturbance

theory assessed how control-surface deflections, structural flexibility, and shock waves in the airflow field interacted. The study also examines the distribution of pressures on the wings. The findings revealed changes in rigid rolling moment calculations, control surfaces' effectiveness, and control-surface reversal patterns as the Mach number transitioned from subsonic to transonic to supersonic regimes. This paper underscores the differences between nonlinear and steady aeroelastic analysis in designing lifting surfaces with deflected control surfaces during transonic flight conditions.

Andersen, Kolonay, and Eastep [20] investigated the utilization of multiple control surfaces for roll control in aircraft. They employed the finite element method to compute structural deformations resulting from consistent aerodynamic input forces generated through a linear panel method. Additionally, the study utilized effectiveness values of control surfaces derived from the stability derivatives related to flexible rolling moments to determine the most efficient control surfaces for achieving specific roll maneuvers. The paper offers valuable insights for thesis research by presenting effectiveness values for various control surfaces. Furthermore, the study examined aircraft models with reduced wing stiffness to assess whether roll performance requirements could be satisfied using multiple control surfaces. It explored the possibility of achieving weight savings while maintaining the desired level of roll performance.

Ricketts [21] described the different tests that can be done on the ground and in the air to identify potential structural issues on aircraft, particularly those on lightweight general aviation airplanes. It lists several structural problems that can occur, such as failure to withstand loads, control surfaces losing effectiveness or moving in the opposite direction, wing twisting and losing stability, and dynamic instability caused by aerodynamic and elastic forces. The paper gives examples of each problem and how the data obtained from testing can be used to predict when they will happen. It also notes that while some general guidelines for predicting structural issues are provided, the report serves as a partial guide for structural analysis. It gives a detailed explanation with clear and easy-to-understand figures.

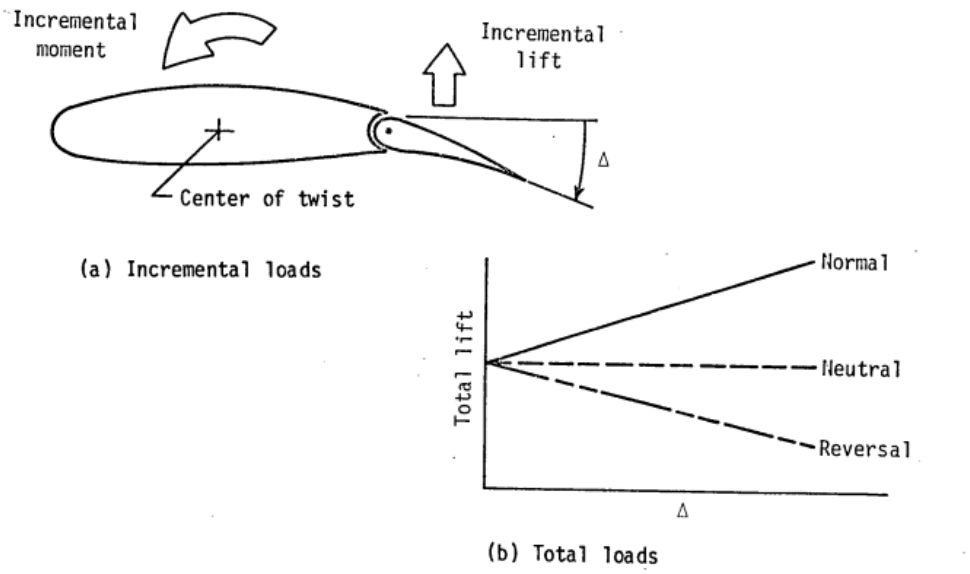

Figure 2.1 Effect of Control Deflection on Wing Load and Moment [21]

The paper also mentioned FAR (Federal Aviation Regulations) Part 23's requirement about the aircraft not having any control reversal throughout its flight envelope, as shown in Figure 2.2. flight testing can prove this requirement that the aircraft does not encounter reversal during its dive speeds. Alternatively, analysis of the aircraft free from reversal up to 40% beyond its cruise speeds or 20% beyond its dive speeds, whichever is lower, can prove this requirement. [21]

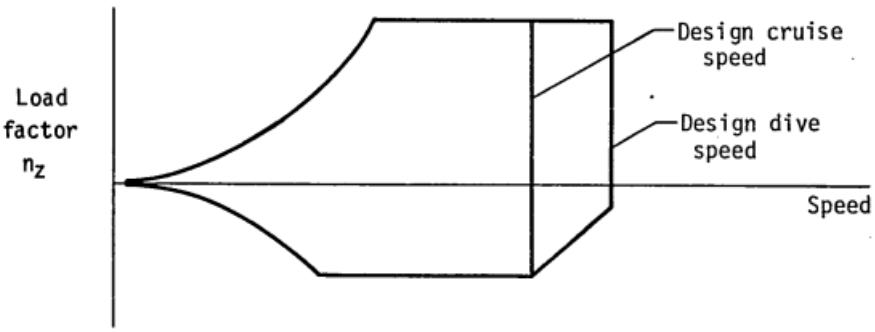

Figure 2.2 Typical Flight Envelope Showing the Relationship between Cruise and Dive Speeds [21]

Mantegazza and Ricci [22] have demonstrated in their research that the study of control reversal can be approached as an eigenvalue problem, and its sensitivity can be determined through a method comparable to the one used for determining the sensitivity of generalized static displacements. This method shows that the control reversal constraint can be integrated into any optimal structural design process. A feasible design can be obtained by uniformly scaling up the design variables.

The paper by Pendleton et al. [23] presented the technical details of their research and provided a summary of the development of their analytical model. Their program aimed to measure and understands the aerodynamic, structural, and flight control characteristics of the aircraft they were studying. The findings of this flight program will be used to provide design guidance for future aircraft designs. The paper suggests that the solution for improvement is integrating control surface allocation with the flight control system rather than making structural and aerodynamic modifications. Additionally, this paper provided valuable information for the study by giving effectiveness values for different control surfaces of aircraft with twin vertical tails.

In their work, Yoon et al. [24] explained the growing significance of understanding the aeroelastic characteristics of aircraft, particularly as they have started to adopt more flexible wing configurations, including high-aspect-ratio wings, and increased flight velocities. Their study underscores the crucial role of precisely assessing the static aeroelasticity of an aircraft, including aspects like control reversal and torsional divergence speed, in ensuring the safety of flights within established operational limits. The paper examines control surface effectiveness and torsional divergence by employing a cross-sectional analysis of aluminum and composite beams and a two-dimensional analysis of aerodynamic coefficients for subsonic-designed airfoils.

In their paper, Rose and Jinu [25] explained that airplane wing structures experience air loads of significant magnitudes from different directions at high-cruising speeds. The flexible wing structure with an elevated aspect ratio produces the bend-twist coupling that often exceeds the control limits, leading to the widespread aeroelastic control reversal issue. This paper investigates the airplane's lateral stability subjected to various aerodynamic forces at cruising flights. They propose a novel idea to find the dynamic stability characteristics of an airplane against the aeroelastic reversal problem. The slope of the wing lift curve, aileron lift curve, and the moment coefficient concerning aileron deflection is computed using computational and experimental methods. The results from wind tunnel testing concurred with the computational fluid dynamics plots and showed that enhancement of the aeroelastic control reversal speed is possible without any significant structural optimization.

In the paper by Qiu and Ang [26], the authors investigated the potential of a new design concept for ailerons that uses both a fixed connector and a moving connector to improve the aileron's effectiveness. They examine how the position of the connector affects various factors such as stress, displacement, load distribution, and control effectiveness. They also investigate how this new design concept affects the wing-aileron connection's stiffness and the aileron's weight. Through analyzing several examples, they conclude that this new concept of aileron design is feasible and provides three different modes for wing-aileron connections as a reference for future study.

Javed and Khan [27] examined the roll effectiveness and reversal of a standard wing by analyzing the static aeroelasticity of a fighter aircraft wing. The analysis uses an analytical model, finite element analysis, and control surface effectiveness measurements to study the structural deformations caused by steady aerodynamic forces and the reversal behavior of the wing structure. An algorithm is developed to analyze the wing, test the effects of different dynamic pressure values, and control surface sizes in an incompressible air environment with a specific dynamic pressure value at zero Mach number. The study aims to develop equations and

methods to improve control effectiveness and prevent control reversal in aircraft wing design.

Schweiger, Weiss, and Kullrich [4] described a new design approach for vertical tails of fighter aircraft that aims to improve their aerodynamic performance while maintaining structural integrity and safety. The approach is based on a smart system for attaching the tail surface to the fuselage, which is first optimized for strength and stability using advanced computational methods. The modifications made to the structural model are then integrated with the active system for attachment. The paper compares this approach to other designs of vertical tails with different shapes. It emphasizes the importance of using efficient multidisciplinary optimization techniques at the early stages of aircraft design. The new approach is expected to result in weight savings, reduced drag, improved stealth characteristics, and reduced loads on the tail structure. The paper also provides insights into how the tail surface's hinge line location and attachment stiffness affects its effectiveness values.

In their work, Nicolosi, Ciliberti, Vecchia, Corcione, and Cusati [28] thoroughly examined design techniques related to aircraft directional stability and the sizing of vertical tails. Their investigation revealed that conventional semi-empirical methods for assessing aircraft directional stability, such as USAF DATCOM and ESDU, may exhibit inaccuracies when applied to specific configurations, mainly due to their reliance on NACA wind tunnel tests conducted on models that do not accurately represent real transport aircraft. Instead of these methods, the authors employed viscous numerical simulations to compute the aerodynamic interactions between various aircraft components across numerous configurations of a typical regional turboprop aircraft. This effort led to the developing of a novel vertical tail design methodology known as VeDSC. The study encompassed both linear and nonlinear regions of aerodynamic coefficients and considered the influence of the fuselage on the vertical stabilizer. Additionally, the paper provided a preliminary exploration of rudder effectiveness in controlling aircraft direction.

In their paper, Singh and Nichols [29] propose a methodology for deriving an equivalent beam for the stabilizer surface of an aircraft. This method aims to make aeroelastic analysis more cost-effective and provide the necessary data for building a wind tunnel model. They have developed an automated interactive graphics procedure that can be used to derive the beam from a detailed finite element model. It is important to note that no single "elastic axis" can be used for all purposes, depending on the structure's support system and loading conditions. However, the equivalent beam can be helpful in specific applications, such as elastic deformation. They also point out that engineering combines both approximation and exact science.

Elsayed, Sedaghati, and Abdo [30] presented a new methodology for accurately predicting the bending and twisting deformations of an aircraft's structure in flight by creating a stick model of the structure. The stick model is a simplified representation of the structure commonly used in aircraft design and multidisciplinary design optimization. The new methodology proposed by the authors improves the accuracy of the stiffness characteristics in the stick model by using a 3D finite element model of the structure to extract the main structure's stiffness properties and apply it to a set of beam elements. The paper compares the proposed methodology to those commonly used in the industry. It validates it by generating a stick model of an aircraft wing-box structure using the proposed methodology and comparing it to a 3D finite element model under the same loading conditions, showing that the new methodology is valid.

Nazar et al. [31] explored control surface effectiveness in reusable launch vehicles, emphasizing lightweight materials like composites in modern aircraft design. Control effectiveness becomes increasingly crucial as control surface weight decreases. This study conducts static aeroelastic analysis on a typical reusable launch vehicle, explicitly focusing on elevon control effectiveness. MSC.Patran™ and MSC.Nastran™ software is used for finite element modeling and analysis, respectively. The primary aim is to assess the launch vehicle's control effectiveness throughout its trajectory. The investigation uses a typical reusable launch vehicle

model for static aeroelastic analysis using MSC.Nastran™ to evaluate elevon control surface performance.

CHAPTER 3

THEORY OF CONTROL SURFACE REVERSAL ANALYSES

3.1 Governing Equations

The thesis study investigates the issue of control surface reversal, the phenomenon where the expected response of the control surface is reversed due to structural deformations in the wing. The loss of control effectiveness poses a significant danger as it can restrict the pilot's ability to control the aircraft in the usual manner. The decrease in control surface effectiveness is especially problematic for aircraft that rely on high maneuverability to accomplish their missions. Therefore, this section focuses on understanding the theory of loss in control effectiveness, which might result in its eventual reversal. For an in-depth understanding of the derivations given in this section, it is suggested that Reference [9] be consulted.

Consider an airfoil section of a wing model that is rigid and uniform spanwise. The example model is designed only to pitch about the support axis, as shown in Figure 3.1. The support is torsionally flexible, restricting the wing's pitching rotation like a rotary spring. The rotational stiffness of the support is denoted by k_t.

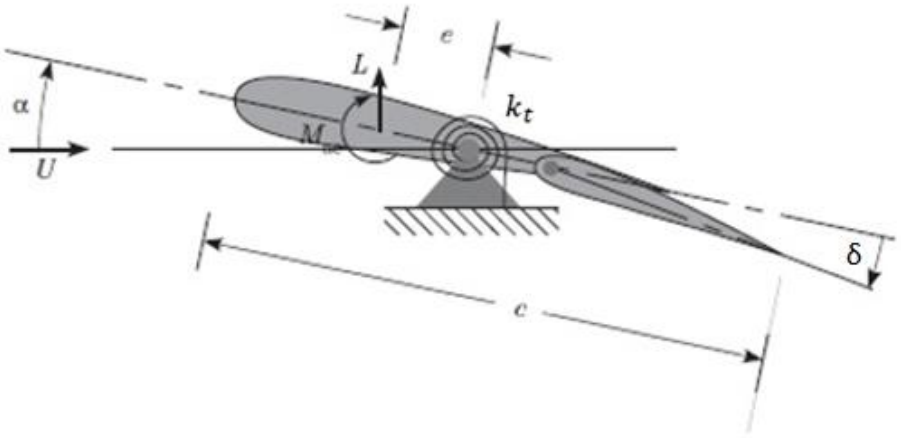

Figure 3.1 Airfoil Section of a Flapped Two-Dimensional Wing [9]

The airfoil has a chord length of c, the angle of attack is denoted by α, and the control surface deflection angle is represented by δ, which the flight-control system can arbitrarily set. The distance between the support and the distance to the aerodynamic center from the elastic axis is shown by e, and the pitch angle is by θ. L denotes the lift generated by the airfoil, and M_{ac} indicates the pitching-moment about the aerodynamic center. The moment equilibrium for this system about the pivot is given as

$$M_{ac} + eL = k_t\theta \tag{3.1}$$

The lift and pitching moment for a two-dimensional wing can be written as

$$\begin{aligned} L &= \bar{q}SC_L \\ M_{ac} &= \bar{q}cSC_{M_{ac}} \end{aligned} \tag{3.2}$$

The dynamic pressure of the air is denoted by the $\bar{q}$ formula with $\bar{q} = \frac{1}{2}\rho_\infty U^2$, where U is the freestream airspeed, ρ_∞ is the freestream air density. S is the reference wing area, C_L is the lift coefficient, and $C_{M_{ac}}$ is the aerodynamic moment coefficient.

When the control surface of the wing is deflected, the airfoil's effective shape changes, which affects both the lift and pitching moment. If the theory used is linear, then both the angle of attack (α) and control surface deflection angle (δ) should be small angles so that

$$C_L = C_{L_\alpha}\alpha + C_{L_\delta}\delta$$
$$C_{M_{ac}} = C_{M_0} + C_{M_\delta}\delta \tag{3.3}$$

where the effective angle of attack is $\alpha = \alpha_{rigid} + \theta$. Noting that C_{M_δ} is negative for convenience, and it is assumed that a symmetric airfoil, C_{M_0} is zero.

The dynamic pressure at which divergence occurs can be determined more directly by formulating the equilibrium equation without considering the inhomogeneous terms. Rewriting Eq. (3.1) by inserting L from Eq. (3.2) gives

$$M_{ac} + eL = k_t\theta$$
$$M_{ac} + e(\bar{q}SC_L) = k_t\theta$$

Inserting C_L from Eq. (3.3) yields

$$M_{ac} + e(\bar{q}S(C_{L_\alpha}\alpha)) = k_t\theta$$

Writing the effective angle of attack as pitch angle rather than the sum of the rigid angle of attack and the pitch angle can be formulated as follows

$$M_{ac} + e(\bar{q}S(C_{L_\alpha}\theta)) = k_t\theta$$

Eliminating the moment about the aerodynamic center term and solution for θ gives

$$(k_t - e\bar{q}SC_{L_\alpha})\theta = 0 \tag{3.4}$$

A non-zero solution can be obtained when the coefficient of θ becomes zero in Eq. (3.4), which provides the value for the divergence dynamic pressure.

$$q_D = \frac{k_t}{eSC_{L_\alpha}} \tag{3.5}$$

It can be seen that the divergence dynamic pressure remains unchanged by the control surface deflection. However, the control surface substantially impacts the pitch angle response. By substituting Eq. (3.2) into the moment equilibrium Eq. (3.1) and utilizing Eq. (3.3), we can solve the pitch angle response problem and obtain the value of θ.

$$\theta = \frac{\bar{q}S[eC_{L_\alpha}\alpha_r + (eC_{L_\delta} + cC_{M_\delta})\delta]}{k_t - e\bar{q}SC_{L_\alpha}} \tag{3.6}$$

It can be observed that the model is flexible in pitch, and θ is also dependent on δ, which is the deflection angle of the control surface. In order to find the lift, firstly, Eq. (3.6) can be substituted into $\alpha = \alpha_r + \theta$ to obtain α.

$$\alpha = \alpha_r + \theta$$

$$\alpha = \alpha_r + \frac{\bar{q}S[eC_{L_\alpha}\alpha_r + (eC_{L_\delta} + cC_{M_\delta})\delta]}{k_t - e\bar{q}SC_{L_\alpha}}$$

Secondly, α can be substituted into the first of Eq. (3.3) to find the lift coefficient.

$$C_L = C_{L_\alpha}\alpha + C_{L_\delta}\delta$$

$$C_L = C_{L_\alpha}\left(\alpha_r + \frac{\bar{q}S\left[eC_{L_\alpha}\alpha_r + \left(eC_{L_\delta} + cC_{M_\delta}\right)\delta\right]}{k_t - e\bar{q}SC_{L_\alpha}}\right) + C_{L_\delta}\delta$$

Finally, the obtained lift coefficient can be substituted into the first of Eq. (3.2) to determine the aeroelastic lift.

$$L = \bar{q}SC_L$$

$$L = \bar{q}S\left[C_{L_\alpha}\left(\alpha_r + \frac{\bar{q}S\left[eC_{L_\alpha}\alpha_r + \left(eC_{L_\delta} + cC_{M_\delta}\right)\delta\right]}{k_t - e\bar{q}SC_{L_\alpha}}\right) + C_{L_\delta}\delta\right]$$

$$L = \frac{\bar{q}S(C_{L_\alpha}\alpha_r\, k_t + C_{L_\delta}\delta k_t + C_{L_\alpha}C_{M_\delta}\delta\bar{q}Sc)}{k_t - e\bar{q}SC_{L_\alpha}}$$

Arranging the term and dividing each term by k_t gives

$$L = \frac{\bar{q}S(C_{L_\alpha}\alpha_r + C_{L_\delta}\delta + \frac{c\bar{q}SC_{L_\alpha}C_{M_\delta}}{k_t}\delta)}{1 - \frac{e\bar{q}SC_{L_\alpha}}{k_t}} \tag{3.7}$$

The expression shows that the lift is influenced by δ in two opposing ways, which can be observed from the two terms in the coefficient of δ. The first term in the numerator that multiplies δ is purely aerodynamic, and increases lift due to a change in the effective camber. The second term is aeroelastic, leading to a decrease in lift due to a nose-down pitching moment induced by the effective change in camber as δ increases. This aeroelastic effect becomes stronger with increasing dynamic pressure. At low speeds, the aerodynamic effect dominates over the aeroelastic effect, and lift increases with δ. However, there is a point where the net change in the lift for δ becomes zero, indicating that the aeroelastic effect has canceled out the aerodynamic effect.

In order to find that point where the net change in the lift for δ becomes zero, the partial derivative of the lift term with respect to β is taken from Eq. (3.7)

$$\frac{\partial L}{\partial \delta} = \frac{\bar{q}SC_{L_\delta}(1 + \frac{c\bar{q}SC_{L_\alpha}C_{M_\delta}}{k_t C_{L_\delta}})}{1 - \frac{e\bar{q}SC_{L_\alpha}}{k_t}} = 0 \tag{3.8}$$

It can be seen that Eq. (3.8) can be used to determine the dynamic pressure value that results in the reversal. This critical value indicates the specific region where the reversal happens.

$$q_R = -\frac{k_t C_{L_\delta}}{cSC_{L_\alpha}C_{M_\delta}} = 0 \tag{3.9}$$

It can be observed that q_R is positive because the conventionally taken value of C_{M_δ} is negative. If we increase the k_t value, the reversal speed will also increase. Furthermore, a rigid wing in torsion will not experience a reversal. Other design

parameters and an evaluation of the sensitivity of the parameters will be presented in Chapter 5. Derivations have been conducted for the pitching degree of freedom; however, it applies to any degree of freedom. This derivation explains the design parameters influencing control surface effectiveness values and reversal point. These parameters will guide the selection of specific design parameters for further investigation, enabling an understanding of their impact on control surface effectiveness and reversal characteristics. At dynamic pressures greater than q_R but lower than the divergence dynamic pressure, an increase in δ will decrease lift. Also, it should be noted that the q_R value is independent of the distance to the aerodynamic center from the elastic axis, as denoted by e, unlike q_D.

3.2 Solution Procedure of MSC.Nastran™

In the thesis study, the SOL144 module of MSC.Nastran™, specifically designed for static aeroelasticity, to investigate the control surface reversal problem. Further details can be found in Reference [33], which explains the solution procedure in MSC.Nastran™.

MSC.Nastran™ enables using any available structural finite elements to construct a model. User input of geometric, structural, inertial, and damping data generates stiffness, mass, and damping matrices for aeroelastic analyses. The aerodynamic influence coefficient matrices are computed from the aerodynamic finite element geometry data. The Doublet-Lattice method (DLM) is applied to the subsonic analysis, which can handle interference among multiple lifting surfaces and bodies. MSC.Nastran™ also includes the ZONA51 method for supersonic analysis, which accounts for multiple interfering lifting surfaces. Aerodynamic grid points are independent of structural grid points.

Static aeroelasticity deals with the interplay of aerodynamic and structural forces on a flexible aircraft, leading to a redistribution of aerodynamic loading with airspeed. The analysis involves interpolating aerodynamic forces from boxes to

structural grid points. The equilibrium equations determine the load distribution and provide information on stability derivatives, trim variables, and loads. The Vortex-Lattice theory (the steady case of the Doublet-Lattice method) is used for subsonic speeds, and the ZONA51 theory for supersonic speeds at zero reduced frequency. The structural analyst is concerned with the resulting changes in internal load and stress and the possibility of static aeroelastic instability. Control surface reversal speed can be found with aerodynamic and control stability derivatives. MSC.Nastran™ calculates aircraft trim conditions and provides aeroelastic stability derivatives to address these issues.

The static aeroelastic equations, given as Eq. (3.10), are essential for fully expressing the equations of motion within the degrees of freedom. For a more comprehensive understanding of the formula, additional explanations are available in Reference [30].

$$[K_{aa} - \bar{q}Q_{aa}]\{u_a\} + [M_{aa}]\{\ddot{u}_a\} = \bar{q}[Q_{ax}]\{u_x\} + \{p_a\} \tag{3.10}$$

Eq. (3.10) is the fundamental equation for static aeroelasticity analysis, including rigid body motions to simulate an aircraft during flight. In this equation, $[K_{aa}]$ is the structural stiffness matrix, and $[M_{aa}]$ is the structural mass matrix generated from the structural finite element model. Depending on the modeling approach, it can correspond to either the consistent mass matrix, which accurately accounts for the mass distribution within each element, or the lumped mass matrix, which simplifies the mass distribution by concentrating it at specific nodes. A consistent mass matrix is generated for the thesis study in the beam-stick model. $\{p_a\}$ is the vector of applied loads calculated using aerodynamic terms obtained from the input of air vehicle speed and downwash velocities from the abovementioned aerodynamic theories. The aerodynamic influence coefficient matrix $[Q_{aa}]$ gives the forces at the structural grid points caused by structural deformations. On the other hand, $[Q_{ax}]$ gives the forces at the structural grid points due to unit

deflections of the aerodynamic extra points. These terms are derived from the aerodynamics finite element model.

The flight dynamic pressure is represented by $\bar{q}$. $\{\ddot{u}_a\}$ is the vector of structural accelerations. The aerodynamic degrees of freedom $\{u_a\}$ and $\{u_x\}$, which represent the structural analysis set and aerodynamic extra points. $\{u_x\}$ vector can be created using predefined variables as input. These variables are incidence angles such as the angle of attack (α) and sideslip angle (β), roll, pitch, and yaw rates (p, q, r), two translational ($\ddot{u}_2$ and $\ddot{u}_3$), and three rotational ($\dot{p}$, $\dot{q}$, and $\dot{r}$) accelerations. In addition, control surface deflections for the aileron, horizontal tail, and rudder (δ_{ail}, δ_{ht}, δ_{rud}) are also taken into consideration as

$$\{u_x\} = \{\alpha, \beta, p, q, r, \ddot{u}_2, \ddot{u}_3, \dot{p}, \dot{q}, \dot{r}, \delta_{ail}, \delta_{ht}, \delta_{rud}\}^T \tag{3.11}$$

The SUPORT card in MSC.Nastran™ is a fictitious support that defines determinate reaction degrees of freedom in a free body. By specifying the desired degrees of freedom output on the SUPORT card, users can control the calculated displacements, rotations, and other structural responses during analysis. This is achieved by partitioning matrices into two sets of degrees of freedom: the r-set for supported degrees and the l-set for left-over degrees. This partitioning scheme enables a focused calculation of the desired output, allowing for a more targeted analysis of specific degrees of freedom relevant to the study. After this partition, Eq. (3.10) becomes:

$$\begin{bmatrix} {K_{ll}}^a & {K_{lr}}^a \\ {K_{rl}}^a & {K_{rr}}^a \end{bmatrix} \begin{Bmatrix} u_l \\ u_r \end{Bmatrix} + \begin{bmatrix} M_{ll} & M_{lr} \\ M_{rl} & M_{rr} \end{bmatrix} \begin{Bmatrix} \ddot{u}_l \\ \ddot{u}_r \end{Bmatrix} = - \begin{bmatrix} {K_{lx}}^a \\ {K_{rx}}^a \end{bmatrix} \{u_x\} + \begin{Bmatrix} p_l \\ p_r \end{Bmatrix} \tag{3.12}$$

where

$$[{K_{aa}}^a] = [K_{aa} - \bar{q} Q_{aa}] \qquad \text{and} \qquad [{K_{ax}}^a] = -\bar{q}[Q_{ax}]$$

When there is a desire to exclude aeroelastic effects, MSC.Nastran™ employs the following mathematical approach. It involves multiplying the first row of Eq. (3.12) by the transpose of $[D]$ and adding the result to the second row, where

$$[D] = -[K_{ll}]^{-1}[K_{lr}] \tag{3.13}$$

The matrix, which is called the rigid body mode matrix, depends only on the model's geometry. The equations that follow are the result of this.

$$\begin{bmatrix} {K_{ll}}^a & {K_{lr}}^a \\ [D^T {K_{ll}}^a + {K_{rl}}^a] & [D^T {K_{lr}}^a + {K_{rr}}^a] \end{bmatrix} \begin{Bmatrix} u_l \\ u_r \end{Bmatrix} + \begin{bmatrix} M_{ll} & M_{lr} \\ [D^T M_{ll} + M_{rl}] & [D^T M_{lr} + M_{rr}] \end{bmatrix} \begin{Bmatrix} \ddot{u}_l \\ \ddot{u}_r \end{Bmatrix} = -\begin{bmatrix} {K_{lx}}^a \\ D^T {K_{lx}}^a + {K_{rx}}^a \end{bmatrix} \{u_x\} + \begin{Bmatrix} p_l \\ D^T p_l + p_r \end{Bmatrix} \tag{3.14}$$

In the absence of aerodynamic terms, the sum of $[D^T {K_{ll}}^a + {K_{rl}}^a]$ and $[D^T {K_{lr}}^a + {K_{rr}}^a]$ would be zero, allowing for the second $\{\ddot{u}_r\}$ row of equations to be solved for easily. However, the presence of aerodynamic coupling makes this simplification impossible. Noting that $[D^T {K_{ll}}^a + {K_{rl}}^a] = 0$ refers to the energy performed on the structure during a rigid body movement.

The unknown accelerations can be defined using two equations. The first equation is based on the assumption of quasi-steady equilibrium and states that

$$\{\ddot{u}_l\} = [D]\{\ddot{u}_r\} \tag{3.15}$$

where $[D]$ is given in Eq. (3.13) and Eq. (3.14) becomes

$$\begin{bmatrix} {K_{ll}}^a & {K_{lr}}^a \\ [D^T {K_{ll}}^a + {K_{rl}}^a] & [D^T {K_{lr}}^a + {K_{rr}}^a] \end{bmatrix} \begin{Bmatrix} u_l \\ u_r \end{Bmatrix} + \begin{bmatrix} M_{ll} D \; M_{lr} \\ m_r \end{bmatrix} \{\ddot{u}_r\} = -\begin{bmatrix} {K_{lx}}^a \\ D^T {K_{lx}}^a + {K_{rx}}^a \end{bmatrix} \{u_x\} + \begin{Bmatrix} p_l \\ D^T p_l + p_r \end{Bmatrix} \tag{3.16}$$

where $[m_r] = [M_{rr} + M_{rl}D + D^T M_{lr} + D^T M_{ll} D]$ is the mass matrix with respect to the u_r points is referred to as the "total" mass matrix. The second relation

acknowledges the relationship between the structural accelerations of $\{\ddot{u}_r\}$ and the aerodynamic extra points $\{u_x\}$ through

$$\{\ddot{u}_r\} = [TR]^T [TRX]\{u_x\} \tag{3.17}$$

The Boolean matrix $[TRX]$ chooses the accelerations from the aerodynamic extra points, while the matrix $[TR]^T$ transforms the accelerations from the aerodynamic reference point to the supported degrees of freedom. The last matrix is dependent solely on the geometry of the model.

CHAPTER 4

AEROELASTIC MODELING OF AN AIRCRAFT HAVING TWIN VERTICAL TAIL

4.1 Model Generation Procedure

The modeling work consists of three distinct phases:

- The creation of the structural model
- The development of the aerodynamic model
- The establishment of the spline relationship between these two models

OpenVSP is an open-source parametric aircraft geometry tool developed by NASA and widely used in aerospace engineering. It allows engineers and researchers to efficiently generate and modify aircraft shapes by inputting specific design details and constraints, making it a valuable tool for creating three-dimensional models. In the modeling studies conducted for this thesis, an Outer Mold Line (OML) representing an aircraft with twin vertical tails was created using OpenVSP. The OML serves as a reference for assessing the dimensions and positions of various components on the aircraft's outer surface. The OML drawing of the specific aircraft used in this study is shown in Figure 4.1, and Table 4.1 provides the design parameters for the model. The OML geometry obtained from reference [34] is the foundation for developing the structural and aerodynamic models in this thesis study.

Table 4.1. External Geometry Dimensions of Twin Vertical Tail Aircraft Model Studied

Design Parameter	Value
Wing Span	11.394 m
Wing Chord (at root)	4.450 m
Wing Chord (at tip)	2.077 m
Length Overall	15.928 m
Tailplane Span	6.199 m

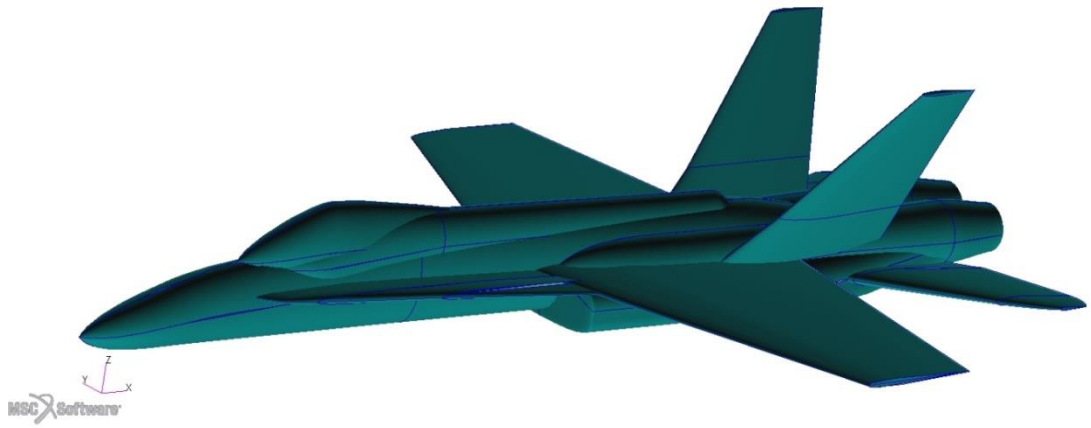

Figure 4.1. OML of an Aircraft with Twin Vertical Tail

4.2 Structural Model

In the structural model of this thesis one-dimensional (1D) beam elements were used. The beam-stick model uses CBAR cards, which define a simple beam element of the structural model. The stiffness of the CBAR element is derived from the Euler-Bernoulli beam theory, also known as the thin-beam or classical beam theory (plane cross sections remain plane during deformation). Euler-Bernoulli beam theory simplifies the complex three-dimensional deformation of an aircraft's wings into a one-dimensional beam-like representation. This simplification is suitable for analyzing static aeroelastic problems such as wing bending and torsion due to aerodynamic loads. A Python code was developed to size the beam elements and create the structural finite element model. Comprehensive information regarding the code constituting the structural model and graphical user interface (GUI) figures can be found in Appendix A.

The code utilized incorporates various procedures to establish the structural model. Initially, the input comprises the start and end coordinates of the aircraft components, including the fuselage, wing, horizontal tail, vertical tail, and control surfaces. Through the linear interpolation, the positions of nodes, which form the basis for creating beam elements, are determined. Subsequently, the sectional lengths of the beam elements need to be specified. These lengths are obtained by measuring the relevant dimensions from the outer geometry using the MSC Patran™ interface. When using the ellipse beam profile, it is essential to input cross-sectional lengths. Inclusion of these parameters is done by providing the wing thickness for the minor axis and the wing chord length for the major axis. These measurements are taken from both the wing's root and tip and then interpolated linearly based on the number of elements to calculate the cross-sectional dimensions of the beam areas. For instance, there is a need to specify lateral lengths when dealing with different components like the fuselage. On the other hand, corresponding chord lengths for each beam element are required for components like the lift and control surfaces. A mesh convergence study

determines the number of beam elements needed for this process. The node positions for these elements are calculated based on the start and end points of the components and the assigned number of elements.

Additionally, the weight distribution of each component is allocated to the elements proportionally, considering the square of the provided sectional lengths. The required cross-sectional area for each element is computed by using the input data on material density to achieve the desired mass. Aluminum material properties were used for the required material density to calculate the required volume for the distributed mass. In addition, the values used for the material properties values required for calculating the stiffness matrix can be found in Table 4.3. Beam lengths are determined according to component length and number of elements. It is used to transition from volume to cross-sectional area, and the cross-sectional length determination process is completed. Subsequently, the second moments of area of inertia are calculated using the sectional lengths of the beam elements. The resulting values, along with the previously determined node positions, are formatted according to the requirements of the MSC.Nastran™ program, creating the PBAR, CBAR, GRID, and MAT1 cards. Consequently, a one-dimensional beam structural model is generated. The flowchart depicting the sequential steps of the Python code responsible for constructing the structural model is illustrated in Figure 4.2.

The aircraft was initially modeled as a half and then mirrored using the Python code to achieve symmetry. This approach is commonly used in aircraft design for cost-effectiveness and simplification of analysis. Symmetry assumption allows for mirroring forces and simplifies computations while modeling only one side reduces redundancy and enables efficient adjustments.

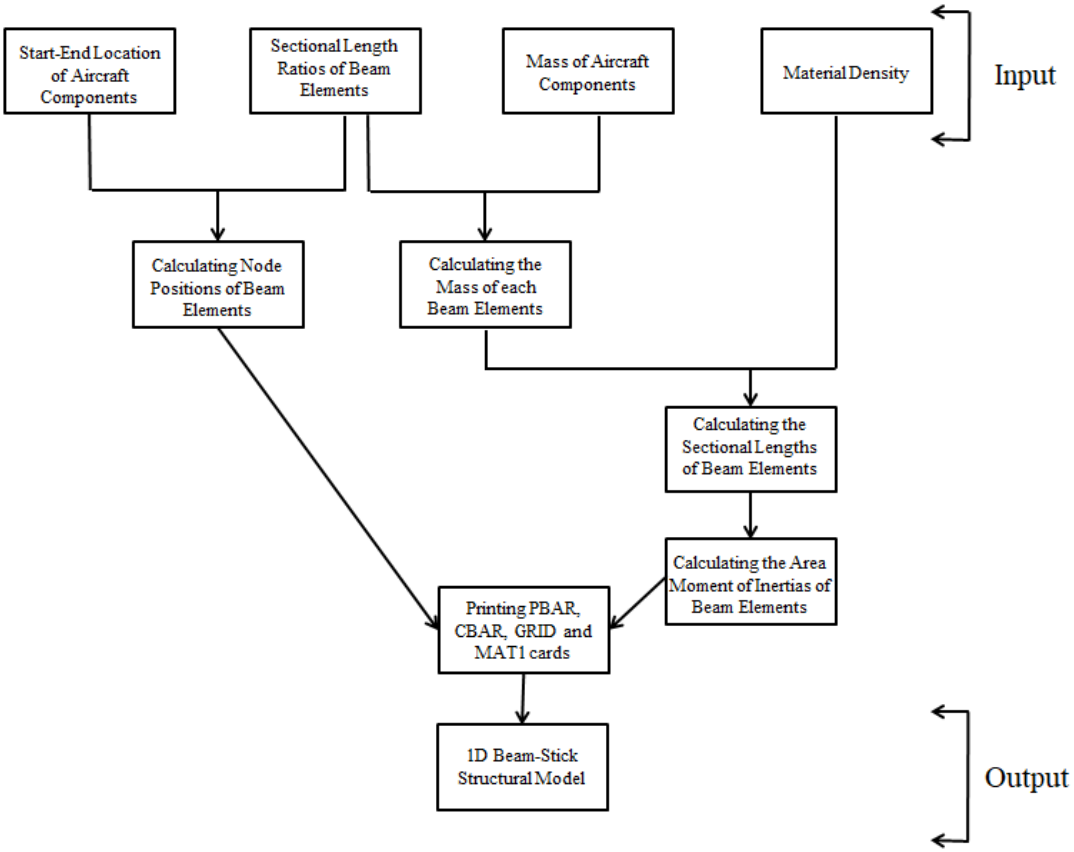

Figure 4.2. Flowchart of Python Code Constructing the Structural Model

A comprehensive mesh convergence analysis is necessary to ensure accurate results. Specifically, a structural mesh convergence study will be conducted for the vertical tail, which holds significant importance in this study, to determine the optimal number of elements and element length. These identified values will subsequently be applied to other components, thereby completing the structural finite element modeling process.

The mesh convergence study for the vertical tail involved varying the number of beam elements, starting with three and gradually increasing up to 90 elements at regular intervals. Displacement values were analyzed to evaluate the bending deflection and torsional deflection. Unit load and moment were applied at the tip node of the vertical tail to assess these deflection characteristics. Based on the

results obtained, the optimal number of elements was determined considering time and accuracy.

To provide a visual representation of the findings, Figure 4.3 illustrates the comparison of bending deflection, while Figure 4.4 presents the comparison of torsional deflection. These figures illustrate the influence of the number of elements on the structural behavior of the vertical tail.

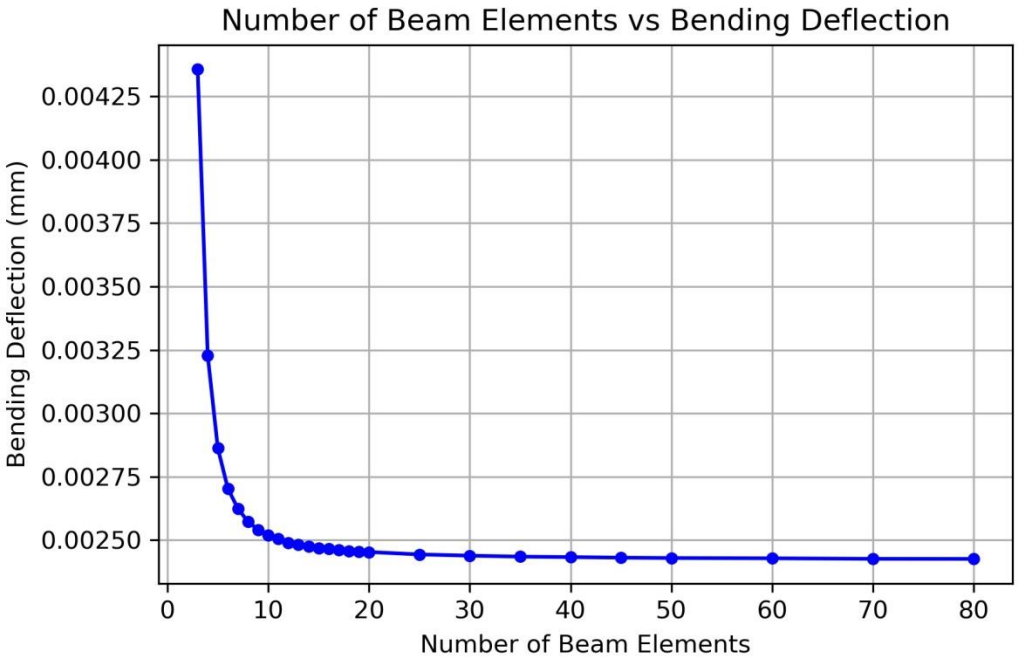

Figure 4.3. Number of Beam Elements vs Bending Deflection

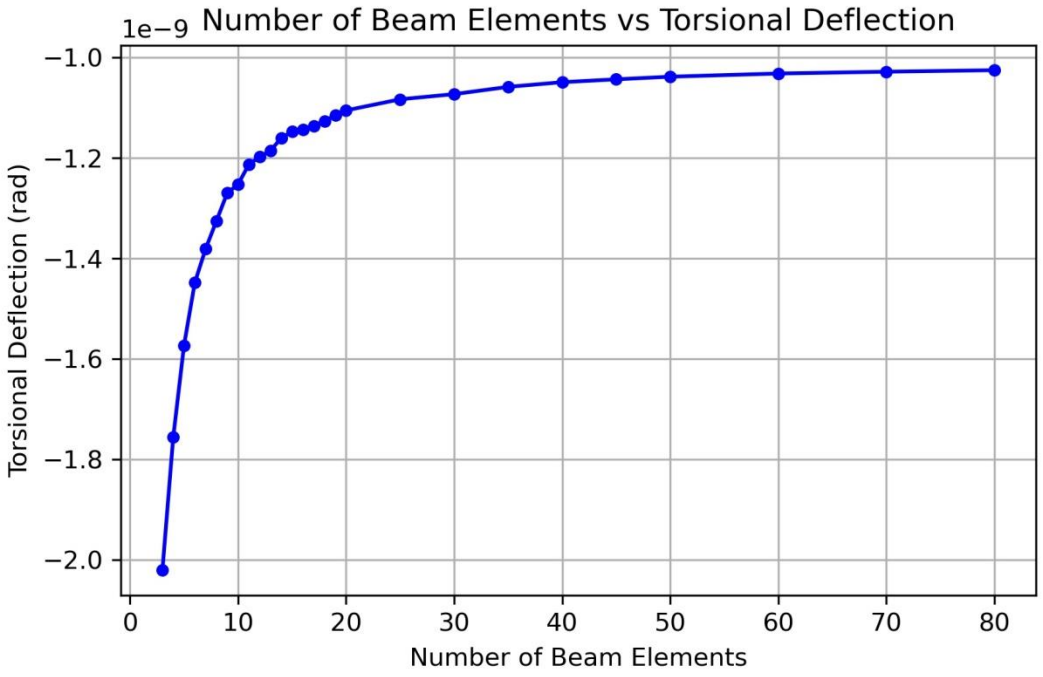

Figure 4.4. Number of Beam Elements vs Torsional Deflection

Following a detailed analysis, considering accuracy and time efficiency, it was determined that a vertical tail consisting of 50 beam elements would adequately represent the desired level of detail in both bending and torsional senses. Subsequently, the structural finite element model was completed by proportionally applying the determined element length and the number of elements to the other components, accounting for their respective dimensions.

Detailed information regarding the structural mass breakdown was required to determine the component masses accurately. This information, resembling an aircraft equipped with a twin vertical tail, was sourced from "Airplane Design" by Jan Roskam [35]. Tables 4.2 and 4.3 provided the necessary input values for completing the structural FE model. The aircraft's mass state consists of only structural mass of around 8010 kg. There is no additional mass modeling for the aircraft like systems, fuels, weapons, pilot, and so on. This makes the creation of a mass matrix is consistent mass matrix from created beams. Since it is a static aeroelasticity analysis, inertia effects are not included in the analysis. A mass

matrix was used in order to create aerodynamic forces and maneuver rates using the quasi-static approach and the trim equation.

Table 4.2. Structural Mass Breakdown Information [35]

Component [Single]	**Mass [kg]**
Fuselage	5912
Wingbox	609
Leading Edge Flap	102
Trailing Edge Flap	68
Aileron	34
Horizontal Tail	106
Vertical Tail	114
Rudder	16

Table 4.3. Material Information Input

Material	**Young's Modulus E [Pa]**	**Poisson's Ratio ν**	**Material Density ρ [kg/m^3]**
Aluminum	7.00E+10	0.35	2.70E+03

In order to ensure the validity of the structural model, a comparison was made between the flexural stiffness (EI) and torsional stiffness (GJ) values of the created vertical tail and a similar aircraft configuration with twin vertical tails [32]. The matching beam profile was determined by utilizing the formulas for the second moments of area of ellipse. The EI-GJ values on spanwise stations were subjected to polynomial fitting in order to provide a better representation of the data and enhance the observation of the trends. The results of this comparison are shown in Figure 4.5.

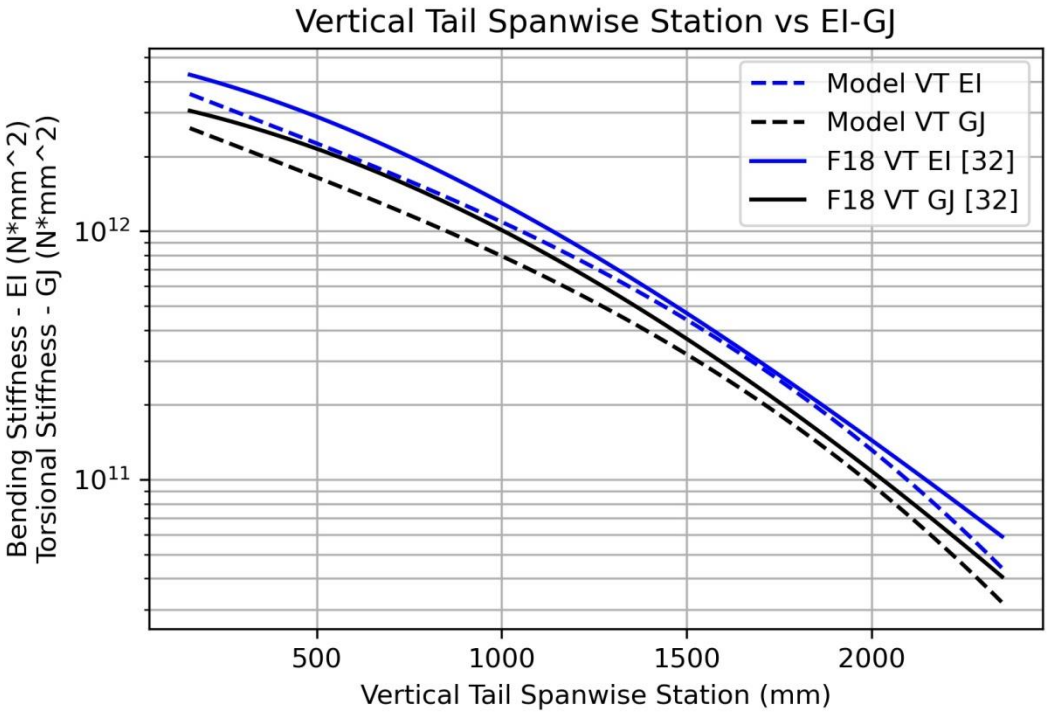

Figure 4.5. Vertical Tail (VT) Spanwise Station vs EI-GJ Values

The structural model has been finalized and comprises of 685 beam elements. These elements have been visually represented in Figure 4.6., with their respective cross-sectional areas, as determined in order to calculate second moment of area values. This visual representation provides a clear overview of the distribution and characteristics of the beam elements in the generic model developed and studied.

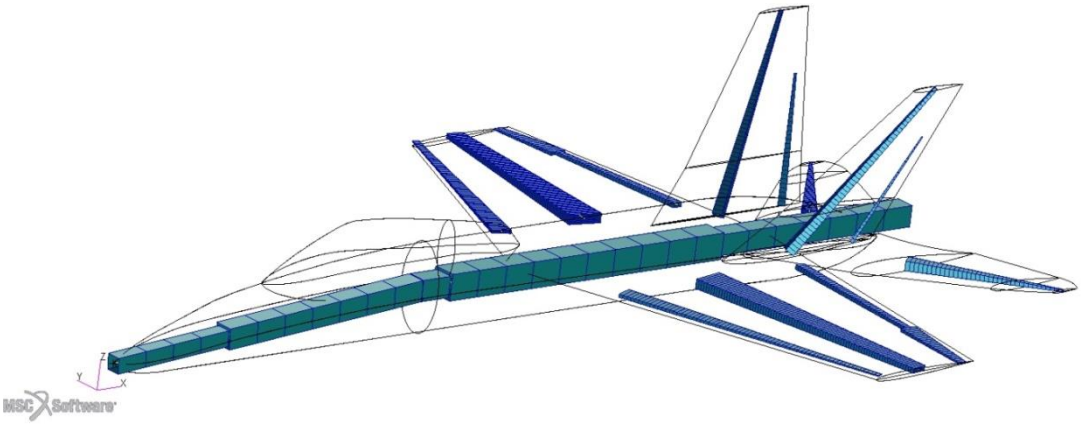

Figure 4.6. Developed and Studied Structural Beam-Stick Model

4.3 Aerodynamic Model

The mesh for the aerodynamic model was created using the MSC Patran FlightLoads™ (FLDS) package program. Two-dimensional elements were used to create the mesh on the surfaces generated by the external geometry drawing. The computation of the aerodynamic influence coefficient matrices is derived from the aerodynamic finite element model and selected method. Since MSC.Nastran™'s aerodynamic solver uses the Doublet-Lattice Method (DLM) for subsonic speeds and the ZONA51 panel method for supersonic speeds, the aerodynamic model must consist of two-dimensional aerodynamic panels.

A mesh convergence analysis is crucial to ensure accurate aerodynamic modeling similar to structural modeling. A study will determine the optimal number of elements and element size for a vertical tail, which is essential in this study. The mesh convergence study for a vertical tail involved systematically varying the number of aerodynamic elements, ranging from 30 to 8670, while maintaining a consistent aspect ratio. Forces and moments were analyzed to evaluate the relationship between side force, aerodynamic moment, and the number of panel elements. The study determined the optimal number of aerodynamic panel elements for a vertical tail and determined element size was applied to the other components after the mesh convergence study.

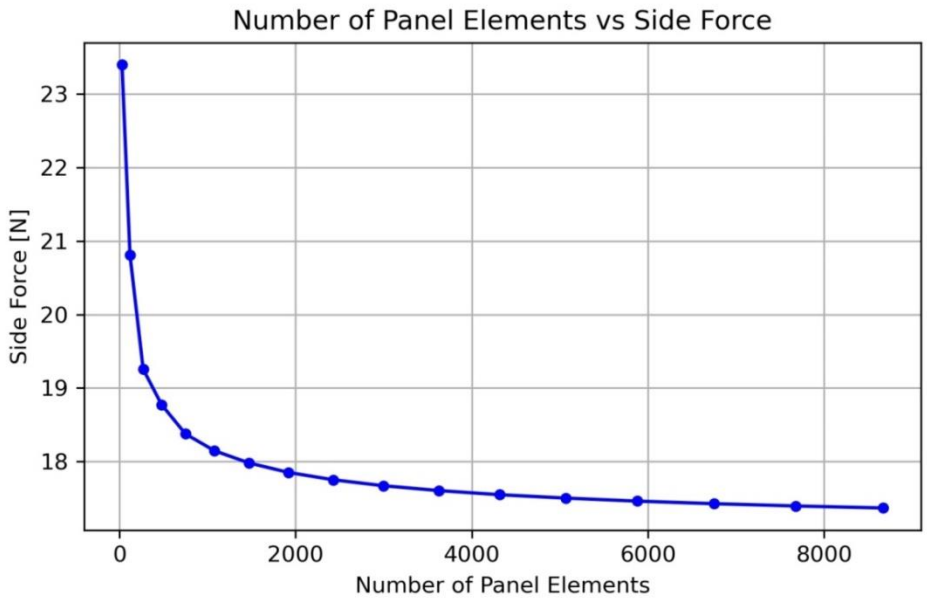

Figure 4.7. Number of Panel Elements vs Side Force Generated

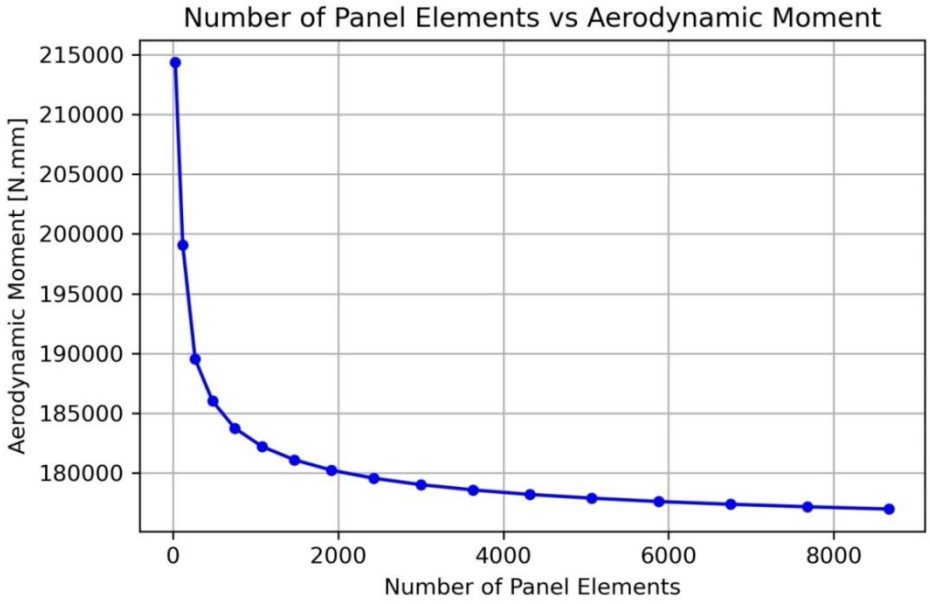

Figure 4.8. Number of Panel Elements vs Aerodynamic Moment Generated

After weighing the balance between accuracy and efficiency, it was found that a vertical tail with around 1500 aerodynamic panel elements would provide the required level of detail. Using this finding, the determined element size and number

of elements were used for the other components of the aerodynamic finite element model, accounting for their dimensions. Detailed information about the code forming the aerodynamic model and the graphical user interface (GUI) images can be found in Appendix B. This led to the finalization of the aerodynamic model, consisting of 6104 aerodynamic panel elements, which can be seen in Figure 4.9.

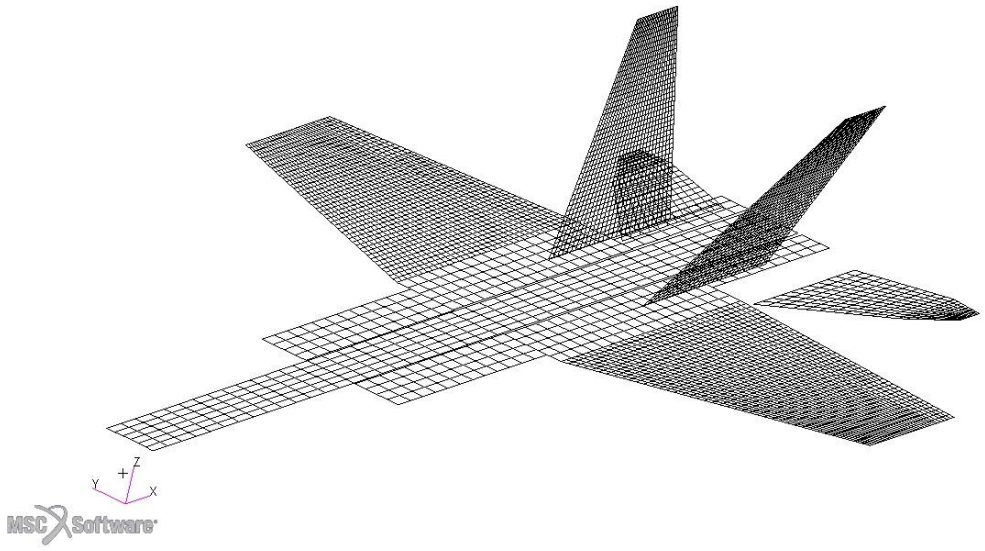

Figure 4.9. Developed and Studied 2D Aerodynamic Model

4.3.1 Full Aircraft Aerodynamic Model

Using a full aircraft model that includes the modeling of the fuselage in static aeroelasticity analysis is crucial for accuracy, as it provides a more realistic representation of the aircraft's geometry and interactions between components. The fuselage affects load distribution and stability assessments, making its inclusion essential for assessing deformations and the overall integrity of wings and tail surfaces. While it adds complexity to the analysis, incorporating the fuselage ensures a more comprehensive representation of the aircraft's aeroelastic behavior in analysis.

A similar study investigates the importance of the aerodynamic model on wing design through aeroelastic tailoring. This research extends the aerodynamic model,

including the fuselage and horizontal tail. The influence of these additions on load distribution and the relative positioning of the aerodynamic center leads to different wing designs. This investigation provides valuable insights into applying a full-aircraft aerodynamic model for optimizing with aeroelastic tailoring. A full aircraft aerodynamic model's wing produces approximately 11% more lift than a wing-only aerodynamics model. Additionally, it is worth noting that full-aircraft aerodynamics exhibit aileron effectiveness values approximately 11% lower than wing-only aerodynamics, confirming this trend [36].

Creating fuselage aerodynamic elements in simulations involving wing and fuselage configurations is essential for accurately modeling their complex interaction. Without the fuselage, the gap between the wing surfaces results in unrealistic vortices at the root wing region. Fuselage aerodynamic elements prevent the generation of these vortices compared to wing-only configurations, enabling a more accurate representation of wing aerodynamic element pressures at the wing-fuselage juncture. Furthermore, to enhance the accuracy of simulation results, it is recommended to model a full aircraft aerodynamic model [37].

A comparative study was conducted to investigate the impact of fuselage modeling on the overall performance of the vertical tail and rudder system. Figure 4.10 illustrates the pressure differences attributed to the presence of the fuselage. It is observed that the inclusion of fuselage modeling results in a remarkable improvement, with a significant 11.5% increase in the total lift generated by the vertical tail and rudder assembly in 0.8 Mach, sea level and, sideslip angle (β) -5 degree given condition compared to the configuration without fuselage modeling.

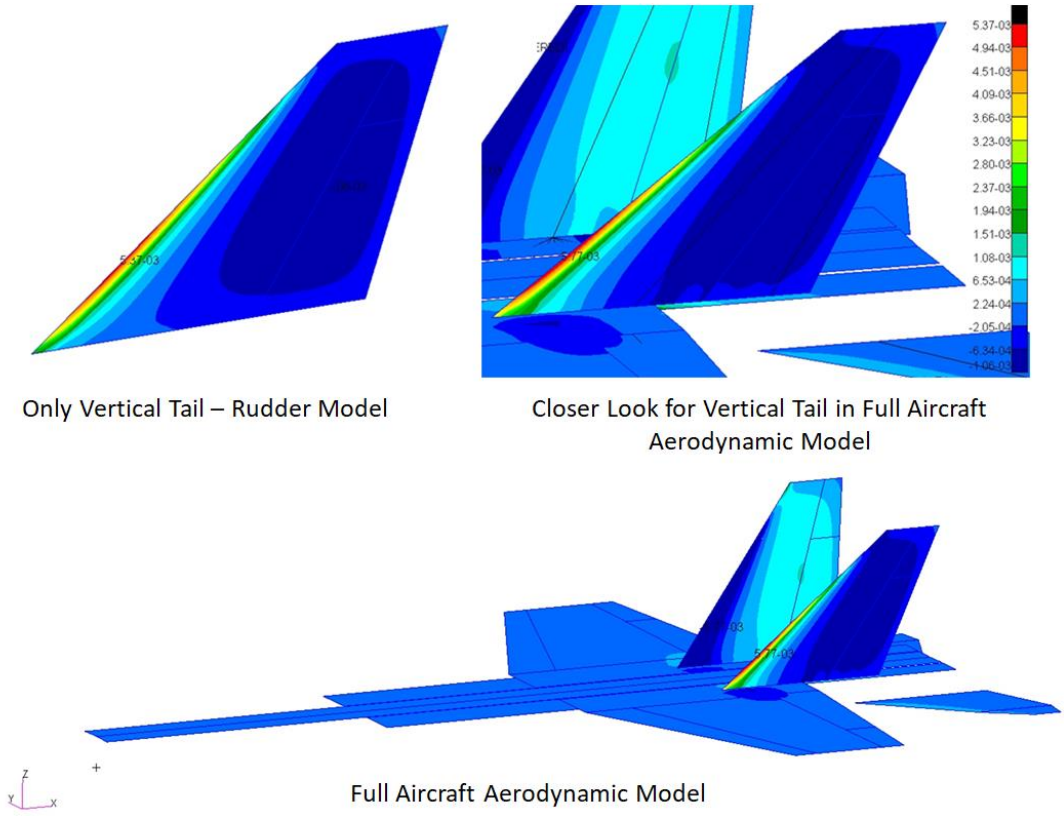

Figure 4.10 Comparison of Pressure Values of Aero Elements for Different Configurations

4.4 Aerostructural Model

Upon completing the aerodynamic modeling process, it is vital to establish a connection between the structural and aerodynamic models to capture their interactions accurately. This connection is facilitated through splines, which enable the transfer of displacements, forces, and moments between the two models. By employing splines as an interpolation method, the aerodynamic and structural meshes are interconnected using an interpolation matrix that relates the deflections of the structural grids to the corresponding deflections of the aerodynamic grids.

MSC.Nastran™ offers a range of spline methods to facilitate linear and surface splines between aerodynamic and structural models. Among these methods, the Infinite Plate Spline (IPS) is commonly employed for coupling aerodynamic and

structural models, mainly when modeling wing-like components. The beam spline method is suitable for high-aspect-ratio wings, while the surface spline method is preferred for low-aspect-ratio wings. The IPS method employs a displacement mapping procedure wherein the initial configuration of the undeformed structural grids is projected onto an infinite plate. By perturbing the grids and conforming them to the surface of the plate, the aerodynamic mesh grids can be positioned on the same plate. Consequently, the aerodynamic mesh undergoes deformation by the displacements of the infinite plate, ensuring an accurate representation of the structural and aerodynamic interactions. Please refer to the reference [30] for more detailed information on this approach.

Nodes in the structural beam-stick model are chosen to establish a correlation with the corresponding aerodynamic nodes. This selection is essential for converting forces and displacements between the aerodynamic and structural models, enabling the accurate transfer of information between the two domains.

According to the Reference [37], the beam spline method requires both transitional and rotational degrees of freedom of the structural grid to compute displacement and forces at the aerodynamic elements accurately. Therefore, ensuring that the structural grids are not given any undesired constraints on their rotational degrees of freedom is critical. While it effectively transfers rotational displacement from the structural to the aerodynamic grid, it does not guarantee the conservation of forces when transmitting rotational aerodynamic forces back to the structural grid. Consequently, beam spline is not recommended for more accurate rotational force calculation and transfer. Instead, users may consider including additional grid points into the structural model and connecting them to the beam structure using rigid elements. They can then employ surface spline methods for accurate calculations in the analyses.

Additional grid points to beam elements are created to ensure a smooth transfer of aerodynamic forces and moments obtained from the IPS method. These supplementary grids are rigidly connected to the selected beam elements'

corresponding nodes, creating a dependable relationship between the aerodynamic and structural models. The aerodynamic panels are chosen to establish an IPS relationship with the relevant structural grids for the coupling process.

The wing and vertical tail components are linked to the fuselage, establishing a structural connection between them. The control surfaces, including the leading edge flap (LEF), trailing edge flap (TEF), aileron, horizontal tail, and rudder, are connected with their assumed actuator stiffness. In Chapter 5.3.4, the study provides a detailed illustration of the connection mechanism and spring element between the main structure and control surfaces. Once the hinge lines are determined for each control surface, these components form the foundation of the base aero-structural model, providing a comprehensive representation of the aircraft's structure and aerodynamic characteristics.

Upon completing this stage, the effectiveness analysis of the base model will be carried out for the thesis study. In the subsequent chapter, the effectiveness values for the base model will be calculated, and a comparison will be made between the yaw effectiveness values influenced by the design parameter values and the base model effectiveness values. This assessment seeks to comprehensively understand the model's behavior by evaluating effectiveness values and examining the impacts of various design variations. After completing the entire aeroelastic model creation process, the model is ready for further research and investigation, as given in Figure 4.11.

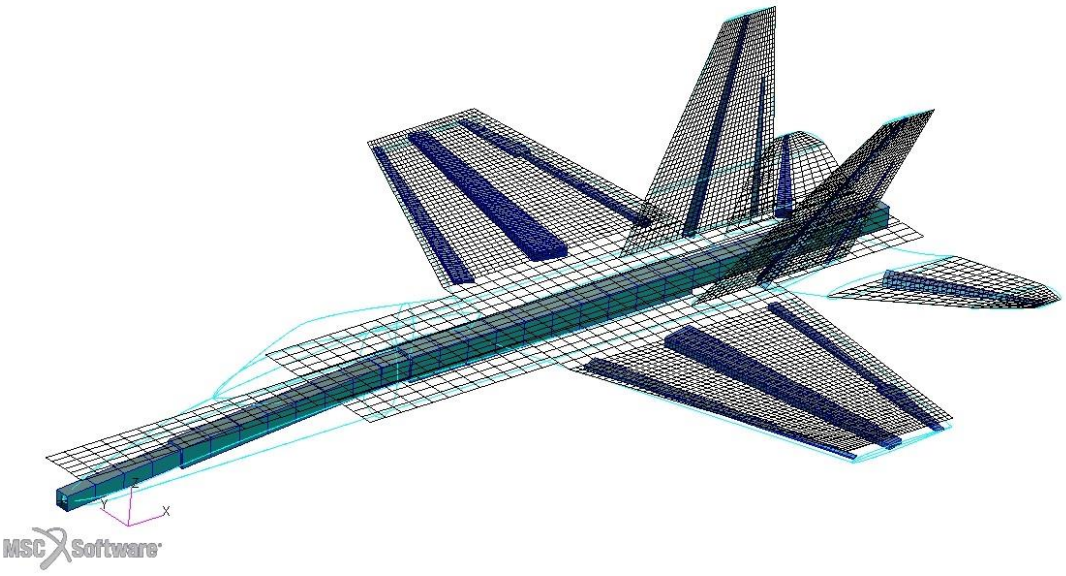

Figure 4.11. Developed and Studied Aerostructural Model

CHAPTER 5

RESULTS AND DISCUSSIONS

In order to assess the effectiveness values of the control surfaces, the flight envelope of the aircraft considered in the thesis was estimated based on the flight envelope of a similar aircraft having a twin vertical tail configuration [38]. Figure 5.1 illustrates the assumed flight envelope to conduct analyses on the selected points, indicated by the orange dots. It is worth noting that the region between Mach 0.9 and Mach 1.1 was excluded (1.0 Mach) from the analysis due to the highly nonlinear behavior of the transonic region. The decision to exclude this range was influenced by the limitations of the MSC.Nastran™ Aero solver is not explicitly designed to model aerodynamic behavior in the transonic range accurately. Addressing the complexities of this region would require a higher fidelity solution, which lies beyond the scope of the thesis study.

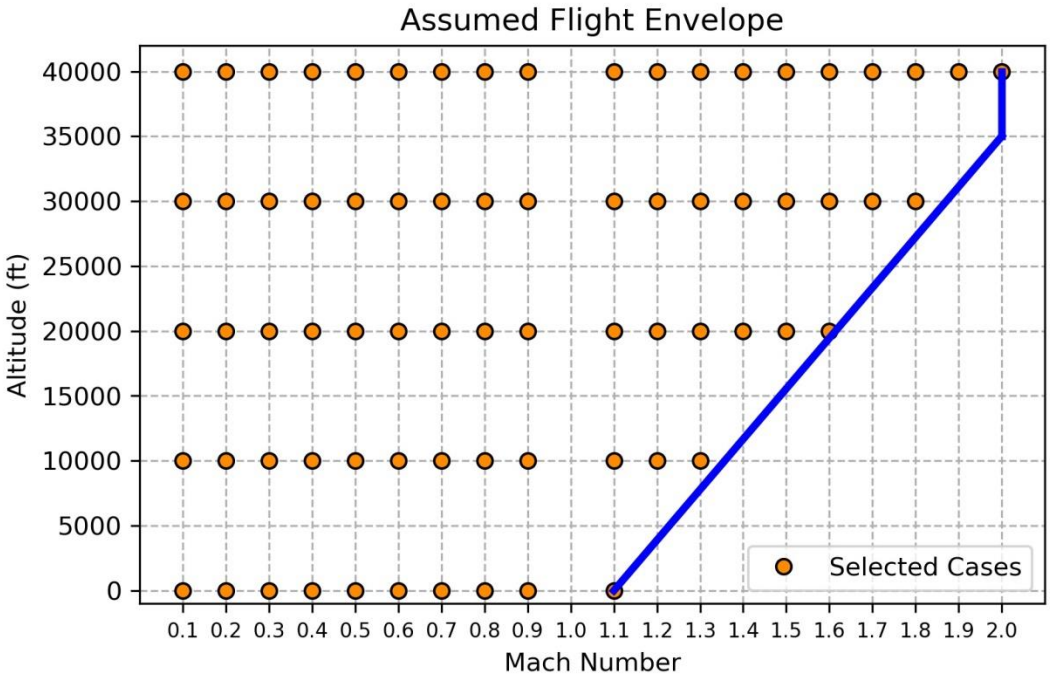

Figure 5.1. Assumed Flight Envelope for Effectiveness Analyses

The dynamic pressure values used for the analysis were calculated using the following equation:

$$\bar{q} = \frac{1}{2}\rho u^2 \tag{5.1}$$

In this equation, $\bar{q}$ represents the dynamic pressure, ρ denotes the density of the air, and u represents the aircraft's speed. The analysis considered the variation in air density across different altitudes and incorporated the corresponding velocity values associated with the Mach number to determine the dynamic pressure for each scenario.

5.1 Aileron and Horizontal Tail Effectiveness Values

While the effectiveness values of aileron roll, horizontal tail roll, and horizontal tail pitch are not considered critical for the thesis work, they are presented for the sake of completeness and to ensure the integrity of the control surface effectiveness analysis. These effectiveness values may provide additional insights and contribute to a comprehensive understanding of the control surfaces' behavior with respect to the aircraft's speed and the influence of the aircraft's flexibility on control derivative coefficients.

The effectiveness value of the antisymmetric roll maneuver will be examined using the ailerons. The analysis was conducted under trim conditions, with the aircraft restricted to five degrees of freedom and allowed to roll only in a single degree of freedom to evaluate the aileron effectiveness precisely. The roll maneuver was performed with an aileron deflection of 0.1 rad (approximately 5.73 degrees). The deflection angle of the control surface is symbolic since the effectiveness is defined as the change in lift per change in control surface deflection for an elastic wing compared to a rigid wing. It can be set to any desired value.

The computation of the aileron roll effectiveness values was carried out by utilizing Equation 1.1, and the calculations were conducted as mentioned above under the flight envelope conditions given in Figure 5.1:

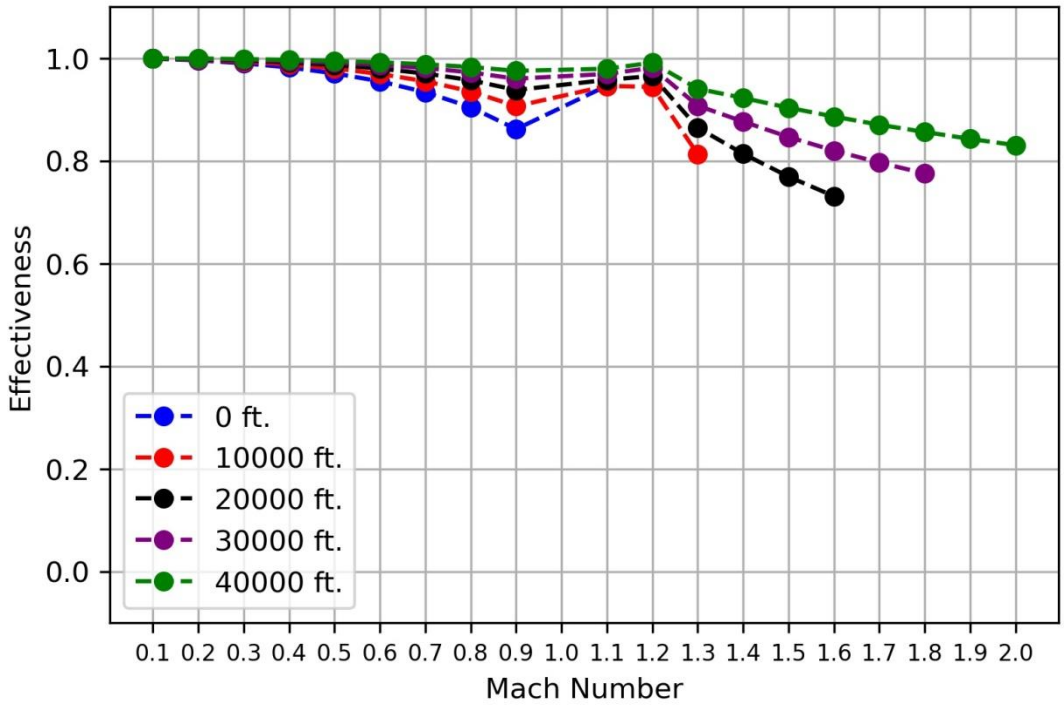

Figure 5.2. Aileron Roll Effectiveness vs. Mach Number

In the subsonic region, it can be seen that the effectiveness of the aileron roll decreases to 86.17% (0.9 Mach, 0 ft.), while in the supersonic area, it diminishes to 73.12% (1.6 Mach, 20,000 ft.) as it can be seen in Figure 5.2. Since the aircraft can fly faster at higher altitudes, primarily because of rarefied atmosphere, higher Mach numbers are only applicable for the increased altitudes. This feature applies to all the other figures involving altitude and the Mach number. Notably, no aileron reversal is observed within the flight envelope. The sudden increases or drops in effectiveness may indicate the occurrence of shock waves caused by the compressibility of the air. Specifically, a shock wave appears during the transition from 0.9 Mach to 1.1 Mach, while it disappears from 1.2 Mach to 1.3 Mach. In order to gain a better understanding of these rapid effectiveness changes, Figure 5.3 illustrates the pressure values on the wing, while Figure 5.4 presents the corresponding deflections resulting from these pressures on both the wing and aileron.

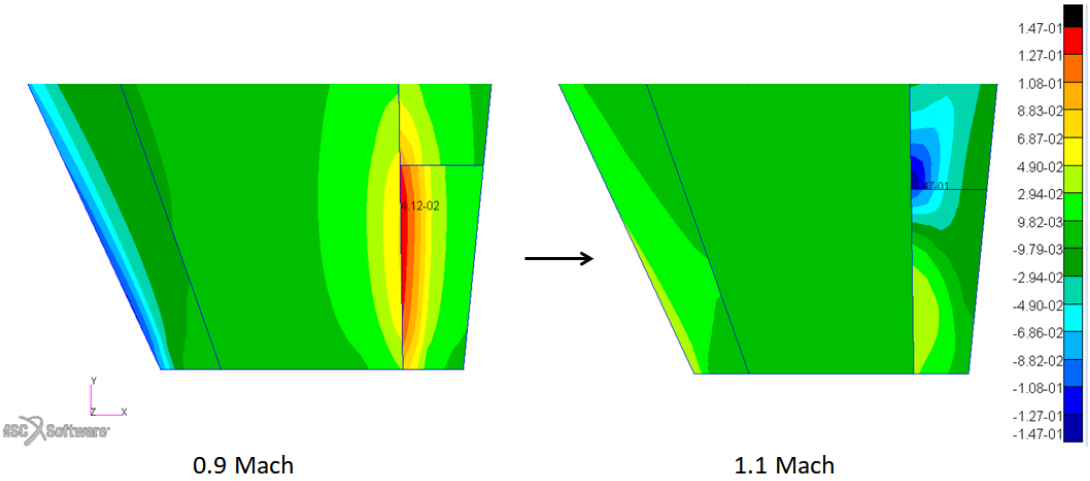

Figure 5.3. Pressure Values of Aero Elements at the Tip of Wing in 0.9 Mach and 1.1 Mach

In the case of negative deflection of the left aileron (where the trailing edge of the aileron is downward), the high-pressure region is expected to be located around the hinge line, as seen in Figure 5.3 for the 0.9 Mach condition. It is essential to highlight that the MSC.Nastran™ Aero solver does not provide separate pressure values on the lower and upper surfaces. This is due to the solver's utilization of two-dimensional aerodynamic panels, which presents pressure values as the difference between the two surfaces. In Figure 5.4, the black grids illustrate the undeformed mesh of the wing's aerodynamic model. At the same Mach number, it can be observed that the resulting lift induces a positive twist, causing a decrease in the effectiveness value. However, at 1.1 Mach, when shock waves occur on the aileron and trailing edge flap (as shown in Figure 5.3, 1.1 Mach condition), a negative twist (the wing's leading edge is upward) is observed, as presented in Figure 5.4 for the same Mach number. Consequently, the additional lift generated by this negative twist increases effectiveness, resulting in a sudden jump in the effectiveness value. As the Mach number goes to 1.3, the effectiveness gradually decreases as the influence of this effect diminishes.

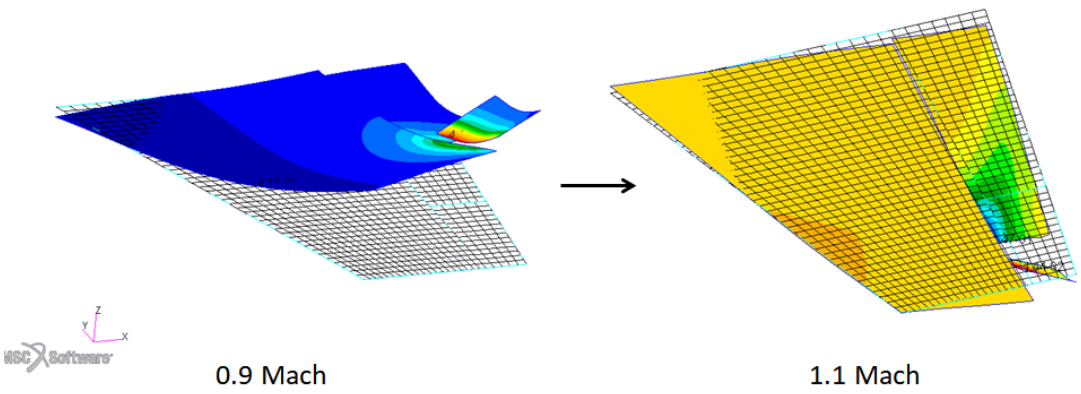

Figure 5.4. Displacements of Aero Elements of Wing in 0.9 Mach and 1.1 Mach

In high-speed flight, the antisymmetric horizontal tail roll maneuver is preferable to the aileron roll maneuver due to its higher loads and relatively lower effectiveness. The effectiveness values for the horizontal tail roll were computed utilizing the assumed flight envelope described in Figure 5.1 and Equation 1.1, with the results presented in Figure 5.5.

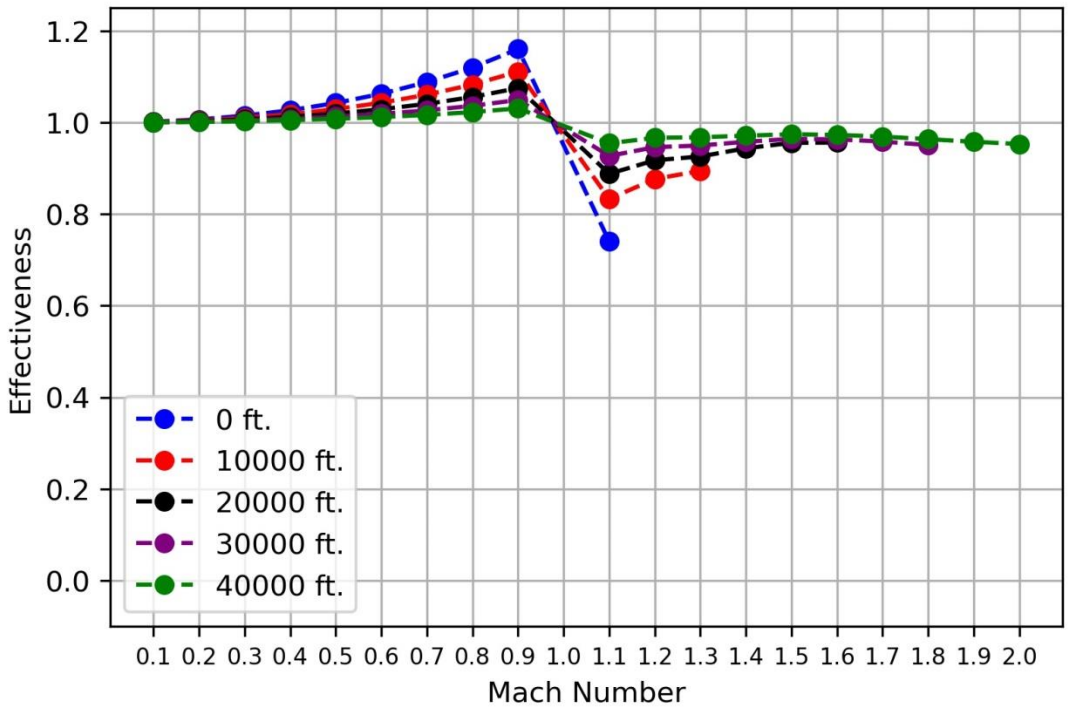

Figure 5.5. Horizontal Tail Roll Effectiveness vs. Mach Number

For all movable control surfaces, such as the horizontal tail, the flexibility enhances the effectiveness value, resulting in values greater than one up until a specific point where the center of pressure shifts from being in front of the elastic axis to behind it. During the transition from subsonic to supersonic speeds, the center of pressure moves from the front to the rear of the elastic axis. This shift leads to a sudden drop in the effectiveness values. In the subsonic region, it is observed that the horizontal tail roll exhibits an effectiveness increase of 116.03% (at 0.9 Mach, 0 ft.). In contrast, in the supersonic region, it decreases to 74.02% (at 1.1 Mach, 0 ft.).

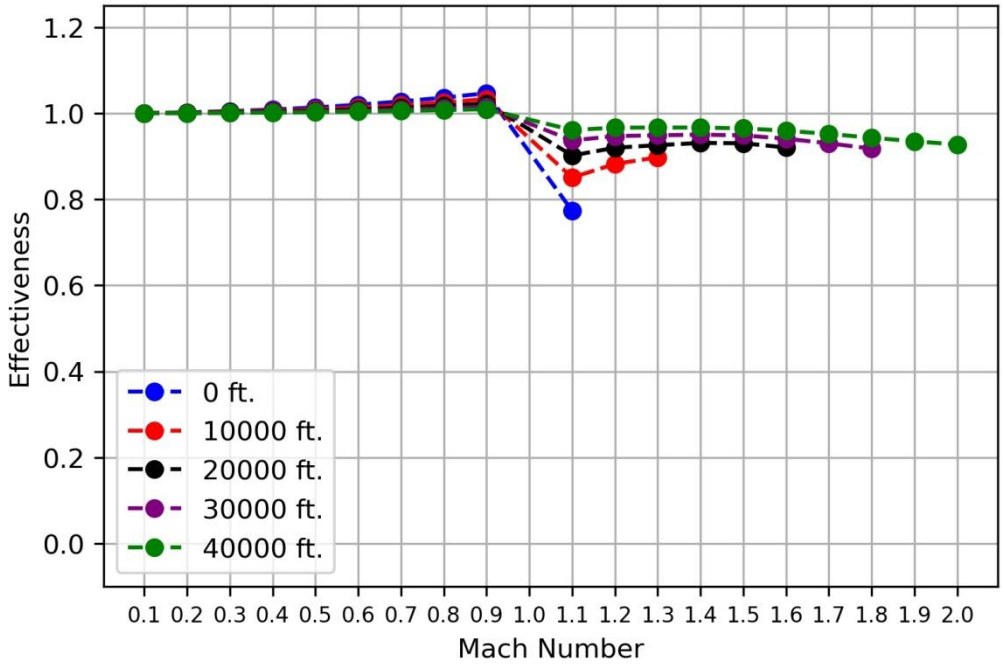

Figure 5.6. Horizontal Tail Pitch Effectiveness vs. Mach Number

The symmetric horizontal tail pitch maneuver exhibits a similar pattern. The effectiveness values for horizontal tail pitch can be found in Figure 5.6. In the subsonic regime, the effectiveness of the horizontal tail roll demonstrates an increasing trend, peaking at 104.65% at 0.9 Mach and sea level altitude. However, as the aircraft transitions to the supersonic regime, the effectiveness gradually declines and reaches 77.35% at 1.1 Mach and sea level altitude.

5.2 Base Model for Rudder Yaw Effectiveness

This section presents the base model values used as a reference for comparing the effects of the investigated parameters using the Design of Experiments (DOE) technique. DOE is a systematic approach to exploring the effects and sensitivity of design parameters. By systematically varying the design parameters within an experimental design, the effects of these parameters can be identified. Comparing the base values with the changed design parameters provides insights for analyzing parameter variations. Figure 5.7 illustrates the vertical tail yaw effectiveness values that will be utilized for the comparative analysis.

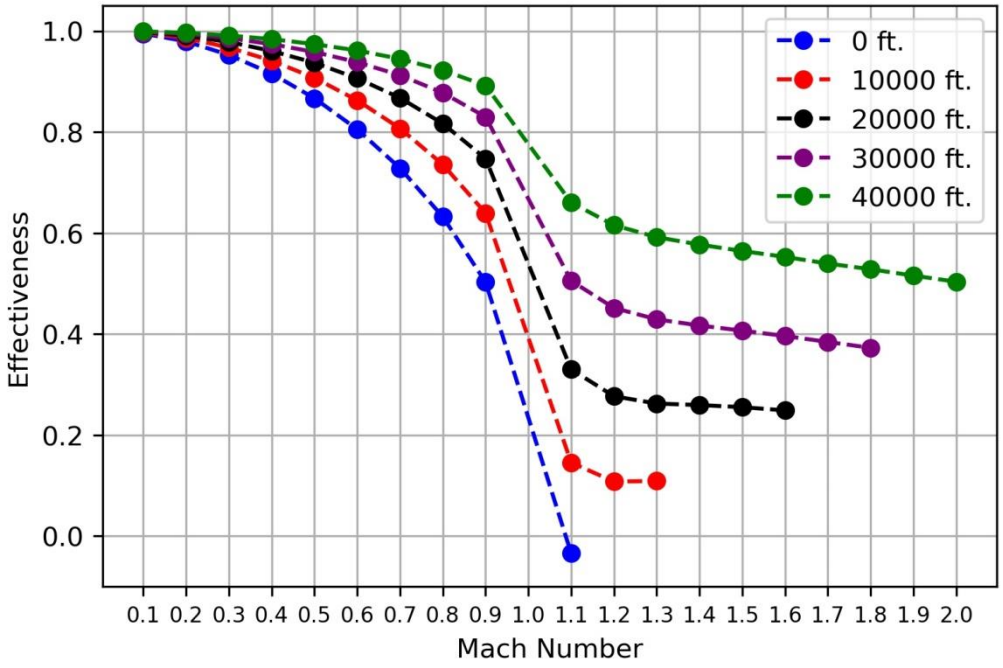

Figure 5.7. Vertical Tail Yaw Effectiveness vs. Mach Number

In the subsonic region, a noticeable decrease in the effectiveness of the vertical tail yaw is seen, with the value dropping 50.27% at a speed of 0.9 Mach and sea level altitude. Moreover, in the supersonic domain, a significant drop to -3.40% is observed at a speed of 1.1 Mach and sea level altitude, indicating a reversal of the control surface at this specific speed.

5.3 Sensitivity Analysis of Design Parameters

In order to address the control surface reversal problem identified in the previous section, this chapter aims to investigate the impact of design adjustments and propose potential solutions. The analysis will primarily focus on the problem occurring at sea level. The design parameters such as torsional stiffness, trailing edge sweep angle, rudder-vertical tail chord ratio, actuator stiffness of the rudder, aspect ratio, taper ratio, and overhang distance will be examined to understand their influence on control surface reversal. These design parameters' influence on control surface reversal can be analyzed, which could result in potential solutions for the detected issue. More detailed explanations of the code that modifies the design parameters and the graphical user interface (GUI) images can be found in Appendix C. Figure 5.8 below clarifies the stiffness values under examination in this study. As shown in the figure, the beam elements for the vertical tail align with the y-axis. Increasing the bending stiffness of the vertical tail requires the update of the second area moment of inertia values, affecting out-of-plane bending movements around the x-axis for all vertical tail beam elements. It is worth noting that this update excludes the values of the spring element used to model the actuator. Figure 5.8 also presents the representative cross-sectional lengths for each element. In modifying the beam properties, the value of each beam element was individually updated to be distributed. While beam elements maintain a constant second moment of inertia values internally, each specific beam element's inertia value differs and is adjusted accordingly, yielding varying stiffness values for the vertical tail. Additionally, when the torsional stiffness value was altered, it included the updates to the second area moment of inertia values along the y-axis. In the case of modifying the actuator stiffness value, only the spring stiffness representing rotational stiffness along the y-axis of the actuator underwent adjustment.

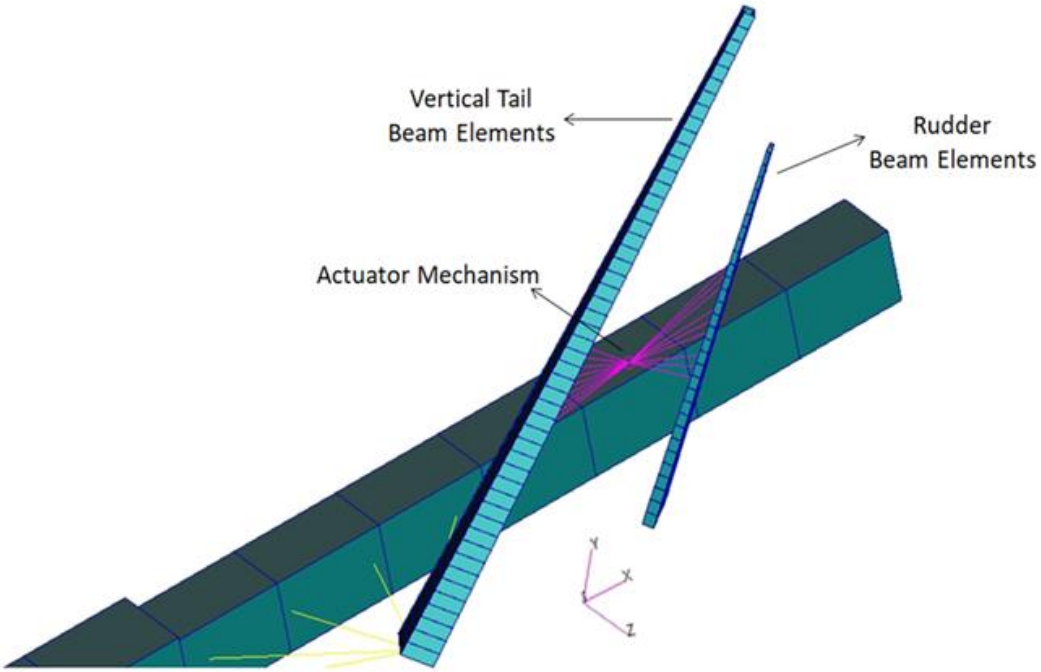

Figure 5.8. Representation for Investigated Stiffness Values

5.3.1 Effects of Torsional Stiffness

Low torsional stiffness has been identified as the primary cause of low effectiveness and other static aeroelasticity issues, such as divergence. In order to loosen the unfavorable effects resulting from twisting and solve the low effectiveness problem, the first design alteration will be increasing the torsional stiffness. The effectiveness problem associated with vertical tail yaw will be assessed by strengthening the vertical tail's GJ (torsional stiffness) values at magnifications of 2, 5, 10, and 100 while keeping the EI (flexural stiffness) values constant. During the examination of the effect of the change, the J values, representing the second area moment of inertia, were updated to evaluate only the GJ values of the vertical tail beam elements. Only the effect of this parameter was intended to be investigated through the design changes. It was assumed that other changes would remain constant. This modification evaluates how enhancing torsional stiffness can resolve the control surface reversal problem.

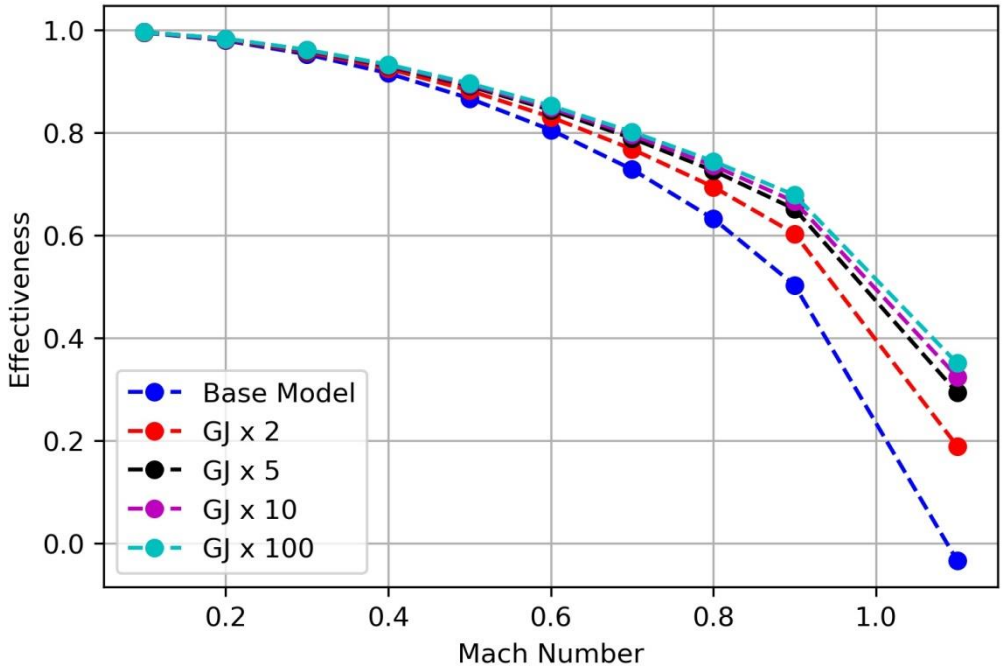

Figure 5.9. Torsional Stiffness Effect on Vertical Tail Yaw Effectiveness

The influence of torsional stiffness on the vertical tail yaw effectiveness and the gradual improvement of the effectiveness value from -3.40% to 35.05% are illustrated in Figure 5.9. The impact of torsional stiffness exhibits an asymptotic effect, meaning it does not enhance additional effectiveness beyond a certain point. The other parameters, such as actuator and rudder stiffness, cause this limitation. Since it would not be possible to increase only the GJ value in the design, the effect of increasing the EI value at the same rate was also examined. In order to achieve further increases in effectiveness, the flexural stiffness (EI) or other design parameters can be changed. The effects of the GJ and EI enhancements can be observed in Figure 5.10.

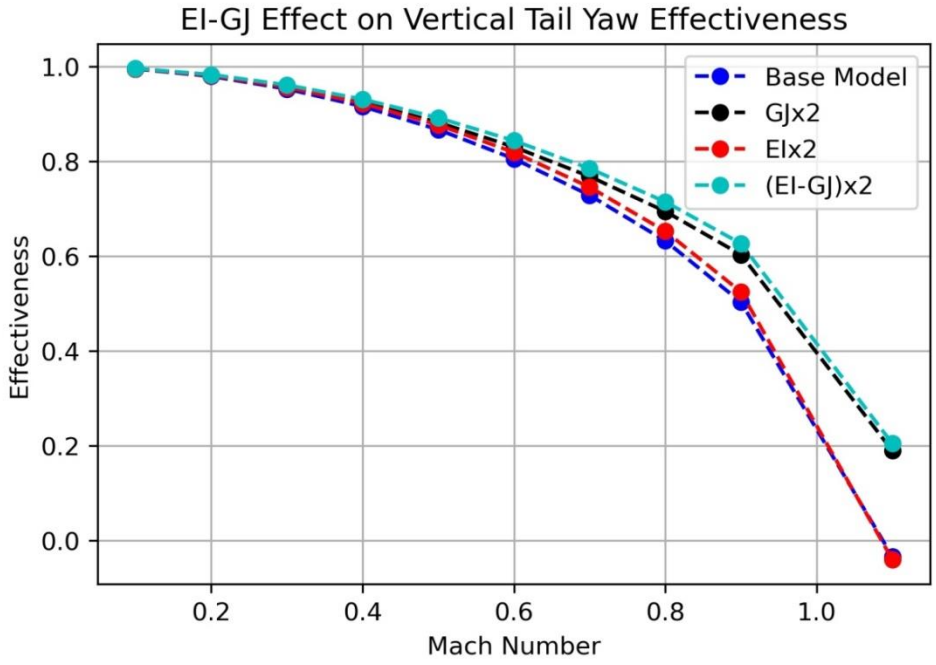

Figure 5.10. Flexural Stiffness (EI) – Torsional Stiffness (GJ) Effect on Vertical Tail Yaw Effectiveness

As observed, the influence of EI on the design is minimal. An increase in EI alone in the region where control surface reversal occurs leads to a lower effectiveness value. As mentioned earlier, design improvements to prevent the twist in the vertical tail effectively enhance the effectiveness value significantly.

5.3.2 Effects of Trailing Edge Sweep Angle

The effectiveness value will increase as the sweep angle of the vertical tail's trailing edge decreases in supersonic region. The base model is initially configured with a trailing edge sweep angle of 11.91 degrees and serves as the benchmark for comparison. Alternative configurations of 0, 5, 15, and 20 degrees are examined to evaluate their effectiveness values, shown in Figure 5.11. In order to assess the impact of the trailing edge sweep angle, modifications were made to the positions of the beam elements, precisely adjusting their starting and ending points. It is important to note that the number of elements and beam properties remained

unchanged throughout this process. Additionally, alterations were applied to the locations of the aerodynamic elements while preserving their quantity. It should be emphasized that all other design parameters were assumed to remain constant during this analysis.

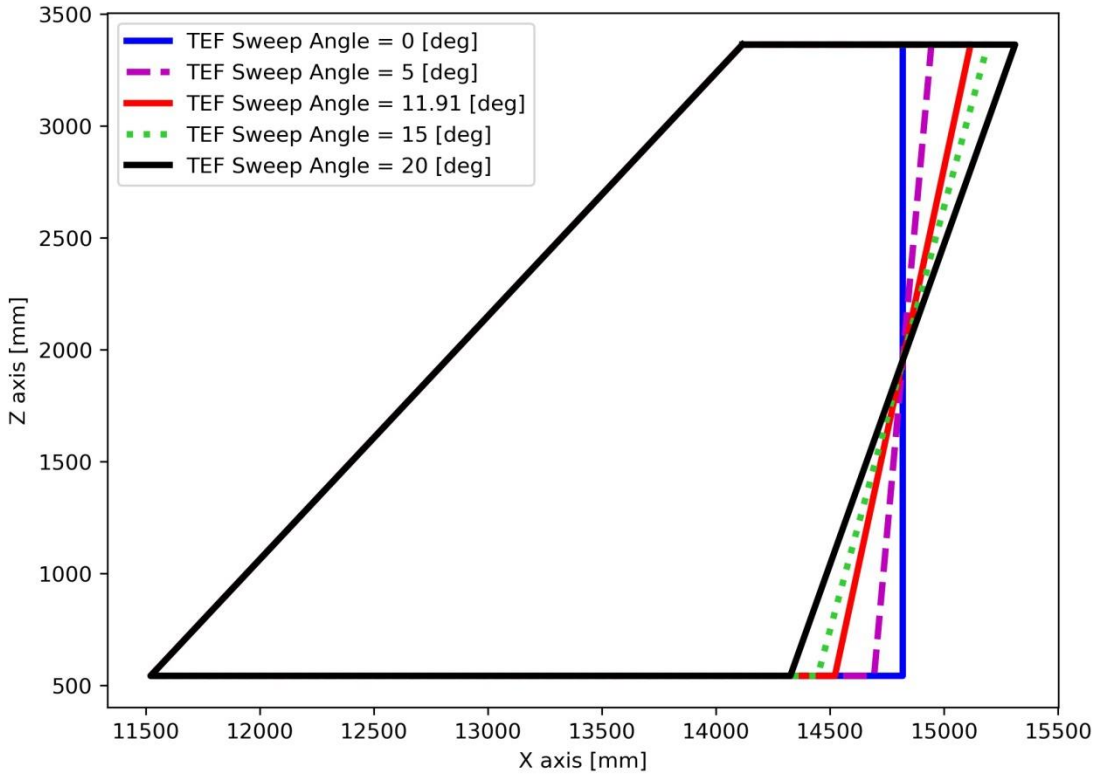

Figure 5.11. Alternative Planforms for Investigation of Trailing Edge Sweep Effect

Figure 5.12 compares the lowest effectiveness values among different configurations, highlighting the impact of a decreased trailing edge sweep angle on the vertical tail. This alteration transforms the torsional moment into a bending moment at supersonic speeds, mitigating high torsional moments in the supersonic speed range. Consequently, there is an increase in effectiveness, an effective modification for addressing the low effectiveness encountered in supersonic conditions.

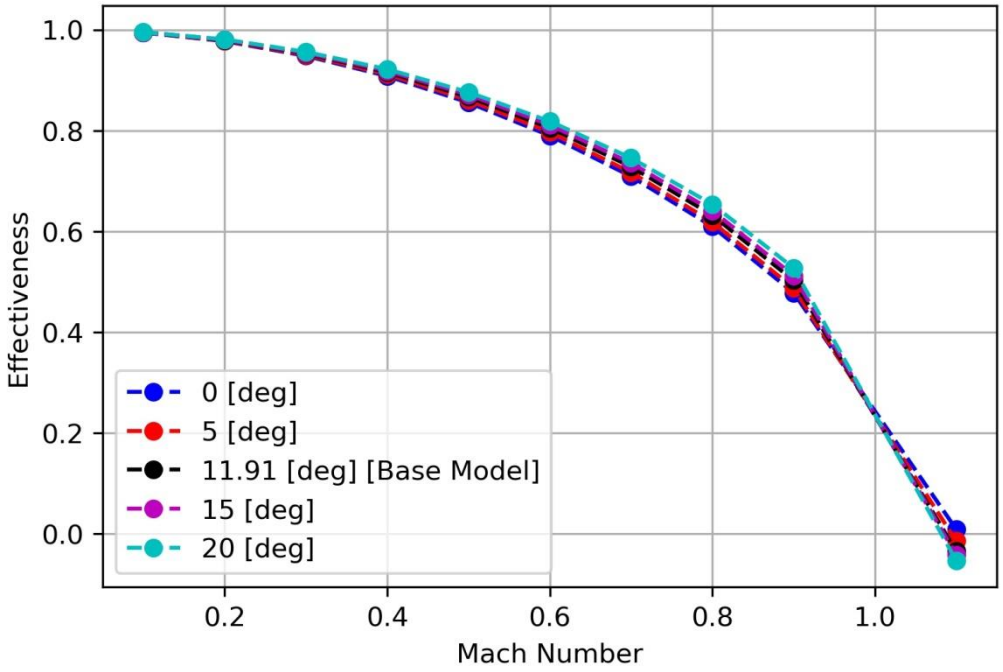

Figure 5.12. Trailing Edge Sweep Angle Effect on Vertical Tail Yaw Effectiveness

When the different configurations are compared, the effectiveness value reaches up to 0.93% in the configuration with a 0 degrees trailing edge angle. However, as the trailing edge angle increases to 20 degrees, the effectiveness drops to -5.28%. It is worth noting that further improvements in effectiveness are expected with higher speeds as the Mach number increases and the center of pressure shifts backward due to air compressibility. When evaluating these values, it might initially seem that altering the trailing edge sweep angle does not significantly impact. However, it is crucial to understand that this design parameter's effect varies across different flight conditions. Specifically, in subsonic flight, where the center of pressure remains closer to the leading edge, changes in the trailing edge sweep angle have a limited influence. In the scenario examined, it is observed that rudder reversal at sea level Mach 1.1 indicates that the design change in this region does not significantly impact the yaw effectiveness values. However, if the rudder reversal situation were to occur at a higher Mach number, a more powerful effect would be expected. This phenomenon is caused by increasing Mach Numbers; due to air

compressibility, the center of pressure tends to shift rearward. It is important to note that this shift is more apparent in higher Mach numbers, and its influence is less noticeable in regions near the speed of sound. Higher trailing edge angles decrease supersonic effectiveness by shifting the center of pressure backward as speed rises. It widens the gap between the center of pressure and the elastic axis. This effect is seen when the supersonic center of pressure is behind the elastic axis and becomes apparent in higher dynamic pressures.

Reducing the trailing edge angle eliminates rudder reversal. However, unlike the supersonic trend, higher angles enhance subsonic effectiveness because the subsonic center of pressure is in front of the elastic axis. Comparing effectiveness values at 0 degrees (47.83%) and 20 degrees (52.75%) at Mach 0.9 proves this. Increased trailing edge angles improve supersonic effectiveness, solve rudder reversal, and affect subsonic yaw performance. Finding the balance of these effects is vital for optimizing aircraft performance across different speed ranges.

5.3.3 Effects of Rudder – Vertical Tail Chord Ratio

It is foreseen that as the chord ratio increases, the control surface forces from the rudder toward the elastic axis will get closer, increasing effectiveness in the supersonic region. In order to examine the effect of the rudder chord ratio, various configurations were compared to the baseline model, with chord ratio values set at 40%, 45%, 50%, and 55%, respectively. Visual representations of the compared vertical tail configurations can be found in Figure 5.13. In order to examine the effect of the rudder-vertical tail chord ratio, the aerodynamic mesh has been updated, as shown in Figure 5.13. In addition, the hinge line, where the rudder is deflected, has also been updated according to the configurations. The spline relationship and control surface definition of newly created or deleted aerodynamic elements have been updated as aerodynamic meshes have changed. Finally, the location of the rudder beam elements and the cross-sectional length of the beam elements were updated. It is assumed that other parameters remain constant.

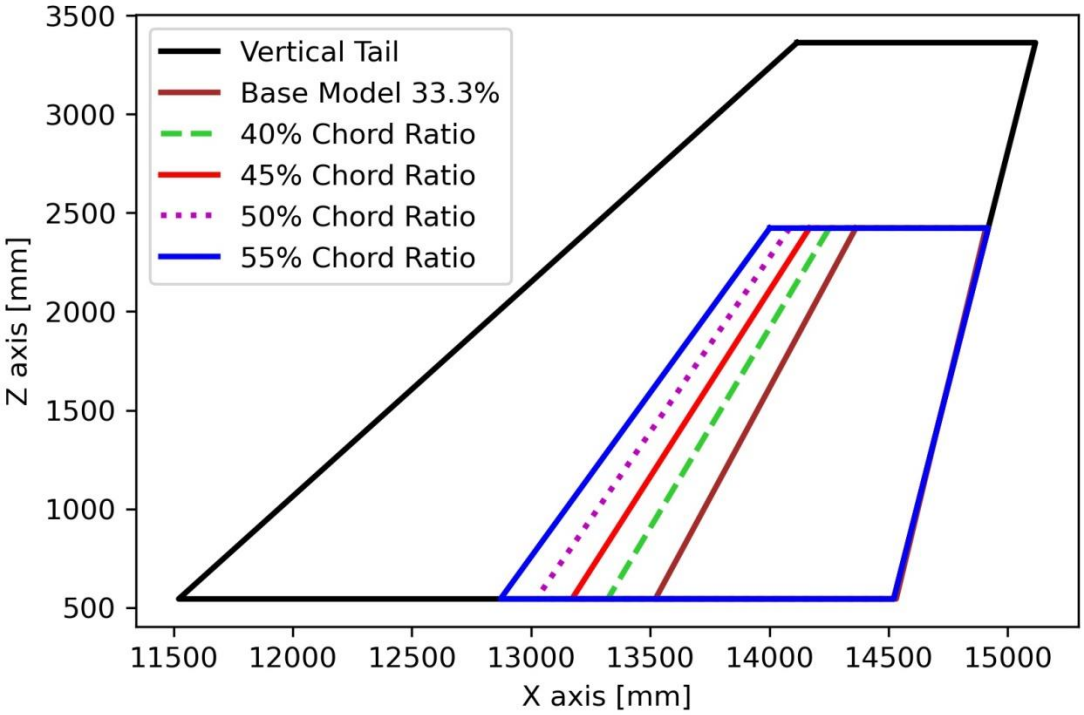

Figure 5.13. Alternative Planforms for Investigation of Chord Ratio Effect

As the aircraft speed and dynamic pressure increase, the reduced distance (due to an increment in rudder chord ratio) between the force generated by the rudder and the elastic axis becomes more significant in the supersonic region, resulting in a positive impact on the rudder's yaw effectiveness. However, this relationship is reversed at subsonic speeds due to the amplified force resulting from the larger rudder surface area. Everything discussed regarding the decrease in the trailing edge sweep angle in the supersonic region also applies in this context. The effect of this design change is that Mach 1.1, where rudder reversal is seen, is less observable when observed at sea level because the speed is very close to the speed of sound. However, if the scenario had been examined at a higher Mach number, a more noteworthy effect might have been observed due to the rudder-chord ratio change. Nevertheless, the magnitude of this effect can vary depending on the specific flight conditions and Mach numbers. Evaluating such design changes in various scenarios is necessary to understand their impact on aircraft performance thoroughly. The problem of rudder reversal encountered at supersonic speeds was

successfully resolved by increasing the rudder chord ratio to 50%, as seen in Figure 5.14. Consequently, the effectiveness value continued to rise in the supersonic region as the rudder chord ratio increased. The rudder yaw effectiveness value initially was at -3.40% in the initial model where rudder reversal was found. However, the progressive increment of the rudder chord ratio reached 5.03% at sea level with a Mach speed of 1.1, effectively eliminating the reversal issue.

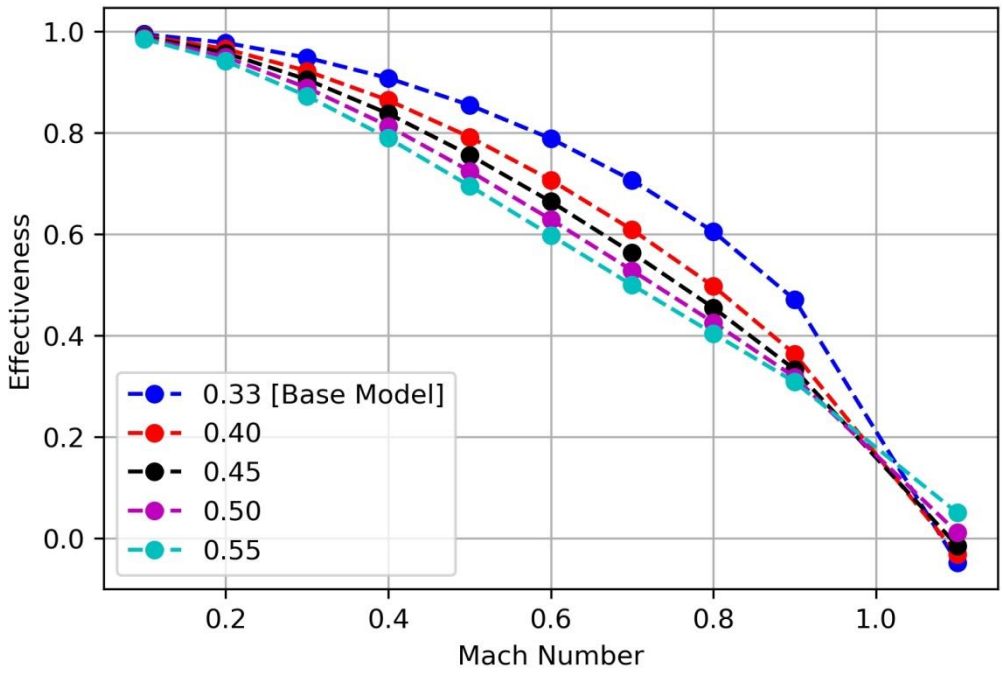

Figure 5.14. Rudder Chord Ratio Effect on Vertical Tail Yaw Effectiveness

5.3.4 Effects of Actuator Stiffness of Rudder

The effectiveness value is expected to increase with an increase in the actuator stiffness parameter. In order to investigate the impact of actuator stiffness, the equivalent rotational stiffness value was reduced by factors of 1/100 and 1/10, respectively, and strengthened by factors of x10 and x100. These configurations were compared to the base model value. The comparison of effectiveness values is

presented in Figure 5.15. In order to examine the effect of actuator stiffness only equivalent rotational stiffness of spring element that connects rudder and vertical tail is changed. Other parameters assumed to stay constant.

Results show the base model achieves 50.27% effectiveness. In comparison, 100 times reinforced case reaches 59.79% at 0.9 Mach, which improves effectiveness if there is no rudder reversal. However, at 1.1 Mach, the base model's -3.40% effectiveness compares to 100 times reinforced case at -5.49%. It is evident that increasing the actuator stiffness value does not resolve the critical condition of rudder reversal; instead, it decreases the effectiveness value. A more detailed explanation of the reason for this situation is given below using Figures 5.17 and 5.18, where the deflection figures of the aerodynamic elements are given. In summary, increasing the actuator stiffness leads to a positive increase in effectiveness if there is no reversal case; however, it does not solve the control surface reversal issue.

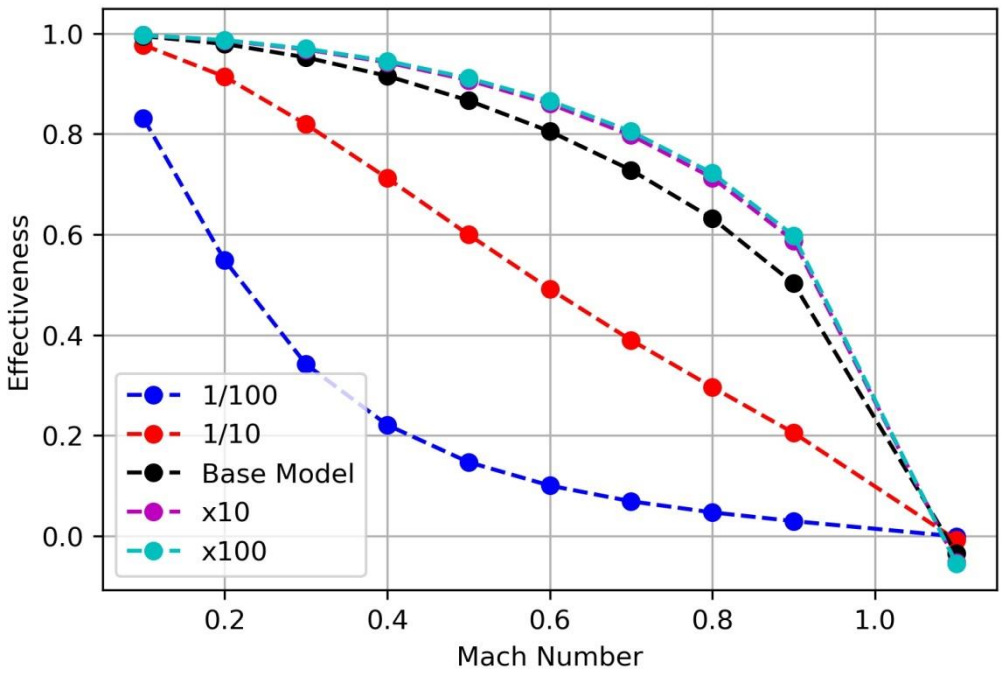

Figure 5.15. Actuator Stiffness Effect on Vertical Tail Yaw Effectiveness

Since only the equivalent rotational stiffness was increased, increasing the actuator stiffness due to the low strength of the rudder did not solve the rudder reversal problem. First of all, the visualization of the actuator mechanism connecting the vertical tail and the rudder is given in Figure 5.16.

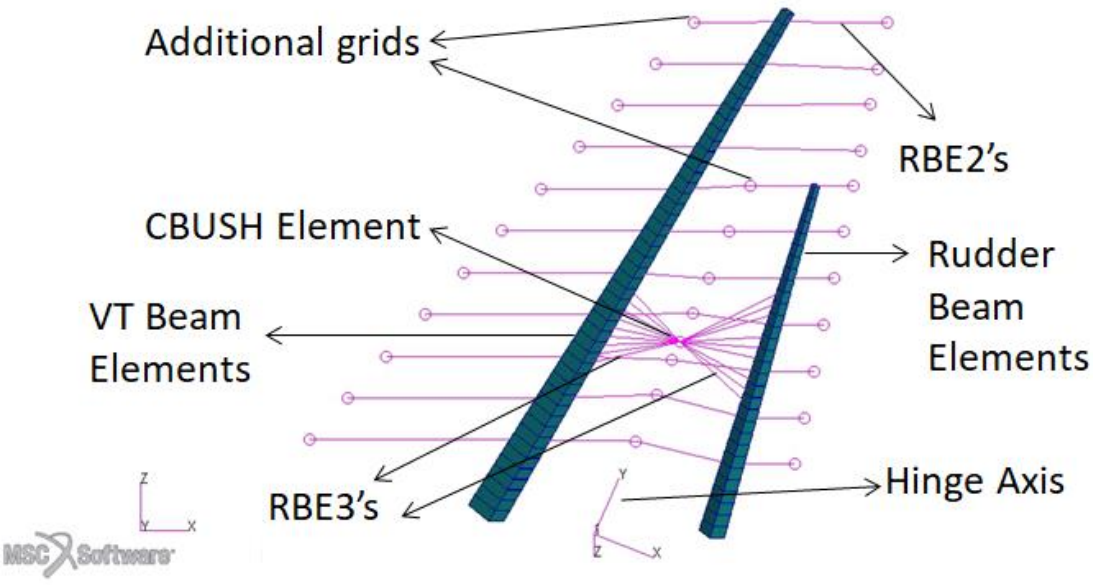

Figure 5.16 Representation of Actuator Mechanism for Rudder

Figure 5.16 shows additional grids with RBE2 rigid connections to enhance surface spline-beam connections, as discussed in Chapter 4.4, Aerostructural Modeling section. MSC.Nastran™ employs the RBE2 element, or Rigid Body Element Type 2, in FE analysis to model rigid connections between two nodes, ensuring they act as a single rigid body. Unlike RBE3, which connects multiple nodes, RBE2 is limited to two-node connections and helps distribute loads or displacements between two nodes.

In Figure 5.16, the left coincident node of the CBUSH element is connected to the vertical tail by the RBE3 element, while the right coincident node of this spring element is connected to rudder beam nodes. The CBUSH element, a spring element in FE modeling, provides translational and rotational stiffness of the actuator system on the hinge axis. The RBE3 element transfers displacements between the main and control surfaces with the corresponding nodes of the CBUSH element. This RBE3 element, also known as the Rigid Body Element Type 3 in Nastran, is a structural element for modeling rigid connections between nodes or grid points in a structural model, allowing connections to more than two nodes, which is particularly useful for complex structures. In Figure 5.16, coincident nodes are positioned at the hinge axis of the rudder, connected to the rudder and vertical tail via RBE3 elements, while the CBUSH element represents an artificial spring. The PBUSH bulk data card assigns the CBUSH element's properties, assigning high stiffness values for translational and rotational axes as connection, except rotational stiffness about the hinge axis (y-axis). This rotational stiffness corresponds to all control surfaces' hinge axis rotational stiffness, giving corresponding actuator stiffness values for each control surface.

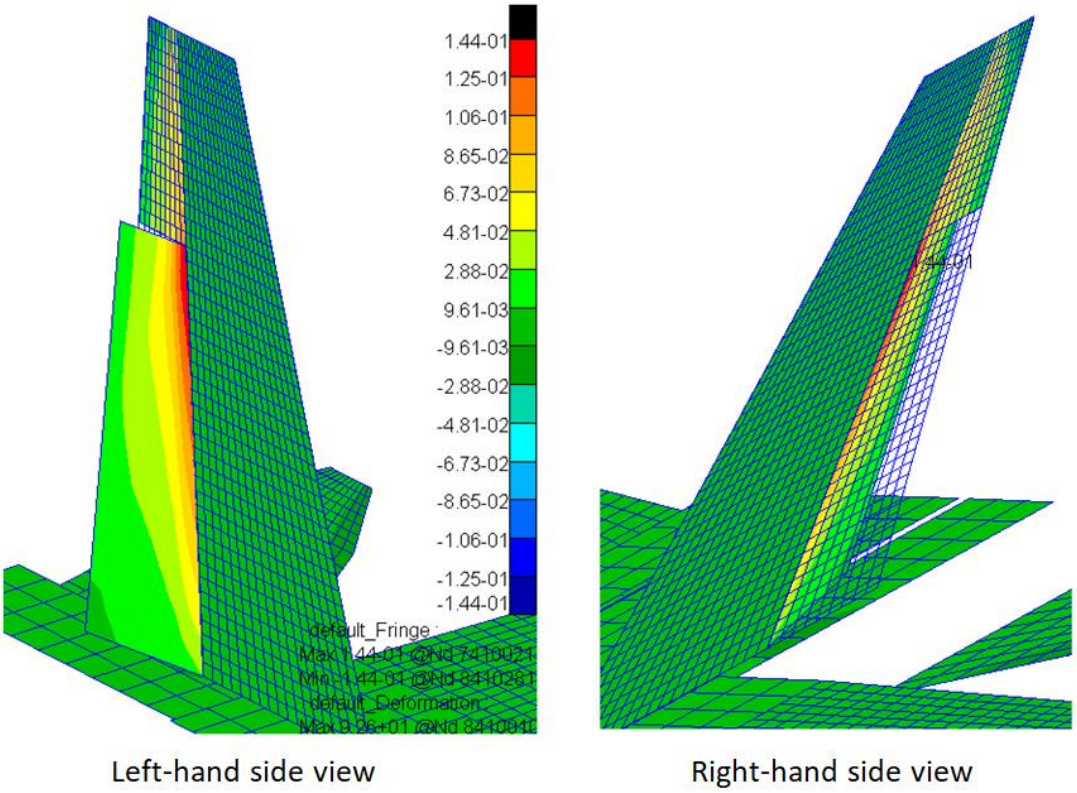

Figure 5.17 Aerodynamic Panel Element Deflections of Configuration of 1/100 Weakened Actuator Stiffness in 1.1 Mach, Sea Level

In the 1/100 weakened actuator stiffness configuration, the actuator connection is highly flexible, so the initial rudder deflection of approximately 5 degrees reverted to its original undeflected position due to the solution with flexible trim. Flexible trim involves iteratively solving solutions up to a specific convergence limit. In order to clarify, the exaggerated panel deflections can be seen in Figure 5.17. The rudder behaved as if it were virtually disconnected, and there was no observable twist in the vertical tail, as evident in the right-hand side view shown in Figure 5.17. In this context, the rudder generated an almost negligible yaw moment. However, it exhibited a negative yaw rate, as evident in the left-hand side view in Figure 5.17, leading to rudder reversal.

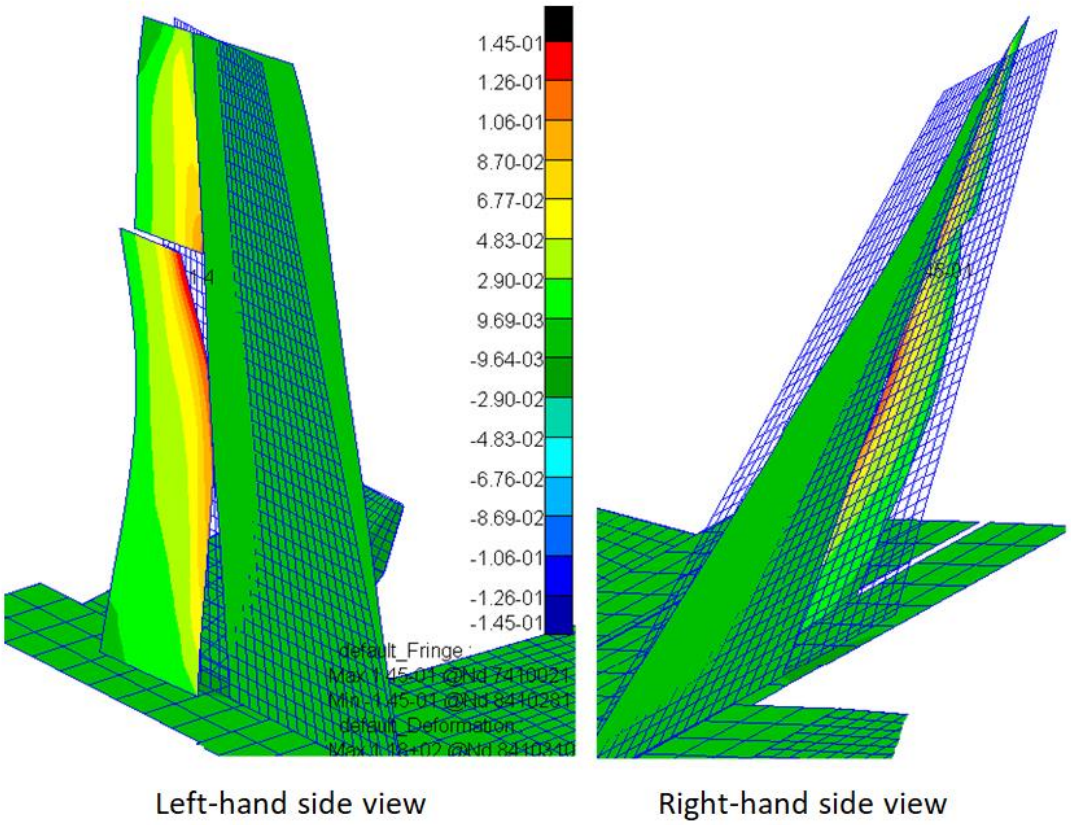

Figure 5.18 Aerodynamic Panel Element Deflections of Configuration of 100 times Strengthen Actuator Stiffness in 1.1 Mach, Sea Level

In the configuration where the actuator stiffness is increased by 100, the actuator connection becomes excessively stiff, causing the vertical tail to twist excessively in response to rudder deflection. In order to illustrate this, the exaggerated panel deflections are shown in Figure 5.18. Despite the significant increase in actuator stiffness, the issue of rudder reversal persists. This phenomenon is primarily due to the rudder twisting and bending excessively due to its inherent lack of strength. Furthermore, the excessive twist in the vertical tail is evident in the right-hand side view presented in Figure 5.18. In this scenario, the rudder generates a negative yaw moment because of its insufficient inherent strength, reflected in its noticeable bending and twisting, as observed in the left-hand side view of Figure 5.18. The right-hand side view of Figure 5.18 also demonstrates that the excessive twist in the vertical tail results in a negative yaw rate. Overall, this configuration yields the

highest generated negative yaw rate and the lowest effectiveness values compared to other configurations, ultimately resulting in rudder reversal at 1.1 Mach at sea level.

In this analysis, the primary focus was on understanding the impact of actuator stiffness while keeping the beam strengths constant. This approach led to the previously mentioned observations. In order to create a more realistic model, the rudder beam elements and vertical tail beam elements to which the actuator is connected will be integrated into the actuator system. The entire system's stiffness will be systematically varied by strengthening it by factors of x2, x5, x10, and x100 of its original value while changing the actuator-connected beam elements' EI-GJ values in the same trend with equivalent rotational actuator stiffness. This approach provides a more representative representation as it considers changes in the EI-GJ values of the connection beam elements, which better reflect changes in the equivalent rotational stiffness of the actuator. The results of these various configurations' yaw effectiveness are compared and presented in Figure 5.19.

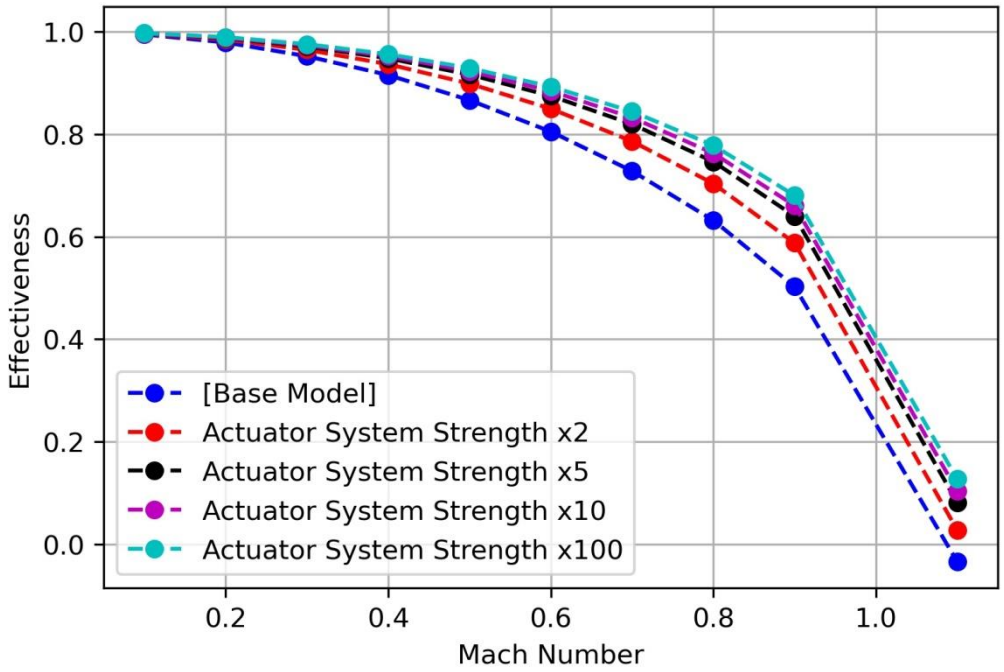

Figure 5.19 Actuator System Strength Effect on Vertical Tail Yaw Effectiveness

Rather than solely altering the rotational stiffness value of the spring element representing the actuator mechanism, a scenario in which the vertical tail beam elements and rudder beam elements to which the spring element is attached are reinforced yields more representative results. This approach is necessary because the spring element, primarily as a connection, cannot prevent the reduction in yaw effectiveness due to the incapability of preventing vertical tail and rudder beam elements from excessive deflections such as bending and twisting. Considering the actuator connection as a complete system encompassing the components linked to the spring element, such as the vertical tail and rudder beam elements, it consistently enhances rudder yaw effectiveness across all speeds, effectively resolving the issue of rudder reversal. It is important to note that this increase is expected to reach a limit at some point due to the influence of other design parameters.

5.3.5 Effects of Aspect Ratio

Reducing the aspect ratio leads to a stronger vertical tail structure. In the case of the vertical tail, the aspect ratio can be changed by adjusting the span length while keeping root and tip chord lengths constant. The calculation formulas for determining the aspect ratio of the vertical tail show slight variations compared to those used for the wing [39]. Equation 5.3 is the general formula for determining the reference area of the wing. It calculates the wing area (S) by multiplying the wing span (b) with the average chord length (C_{avg}), which is calculated as the average of the chord length at the root of the vertical tail (C_r) and the chord length at the tip of the vertical tail (C_t).

$$S = b\left(\frac{C_r + C_t}{2}\right) \tag{5.3}$$

The aspect ratio formula commonly used for wings can also be applied to vertical tails, as indicated by Equation 5.4.

$$AR_{VT} = \frac{b^2{}_{VT}}{S_{VT}} \tag{5.4}$$

In the context of vertical tails, the aspect ratio calculation is based on the span from the root to the tip, represented by the height of the vertical tail (b_{VT}) from its base to the tip. It is important to note that the span from the tip to the tip is not meant for vertical tails. Combining Equation 5.3 and Equation 5.4 gives:

$$AR_{VT} = \frac{b_{VT}}{C_{avg}} \tag{5.5}$$

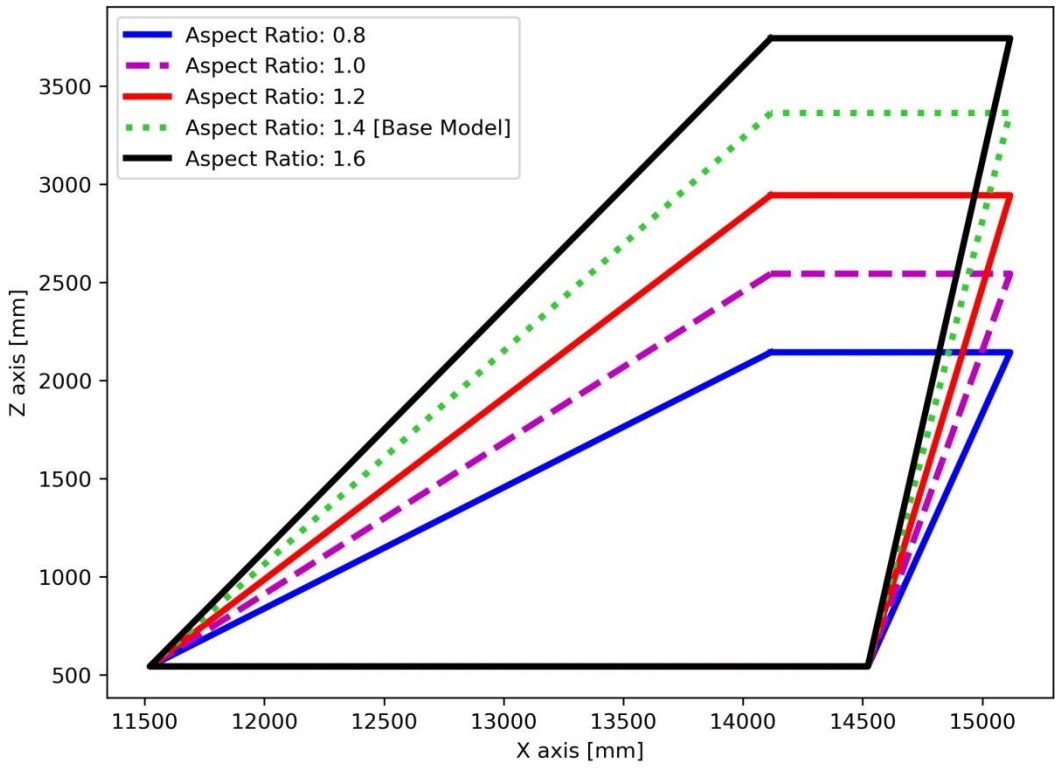

Figure 5.20. Alternative Planforms for Investigation of Aspect Ratio Effect

A stiffer vertical tail is obtained as the aspect ratio decreases, resulting in higher effectiveness values. In order to examine the effect of the design parameter change, the vertical tail aerodynamic model was modified to represent the planforms shown

in Figure 5.20. Furthermore, the vertical tail beam elements were resized to ensure that the component's weight remained unchanged, and their locations were adjusted accordingly. This change leads to the obtaining of an inherently reinforced vertical tail structure. As illustrated in Figure 5.21, enhancements in yaw effectiveness were observed across all speeds, and the problem of rudder reversal was successfully addressed. These improvements highlight the effect of aspect ratio on yaw effectiveness values. At the highest aspect ratio of 1.6, the effectiveness value is as low as -21.48% at 1.1 Mach and sea level conditions. On the other hand, the lowest aspect ratio of 0.8 yields significantly higher effectiveness, reaching up to 42.45%, as seen in Figure 5.20. In the configuration with an aspect ratio of 1.0, a high-pressure zone is observed in the rudder area when operating at Mach 0.9, resulting in a sudden decrease in the effectiveness value. Although a higher fidelity computational fluid dynamics (CFD) solution should be conducted to analyze the shock, it should be noted that this analysis is beyond the scope of the current study and does not impact the obtained results.

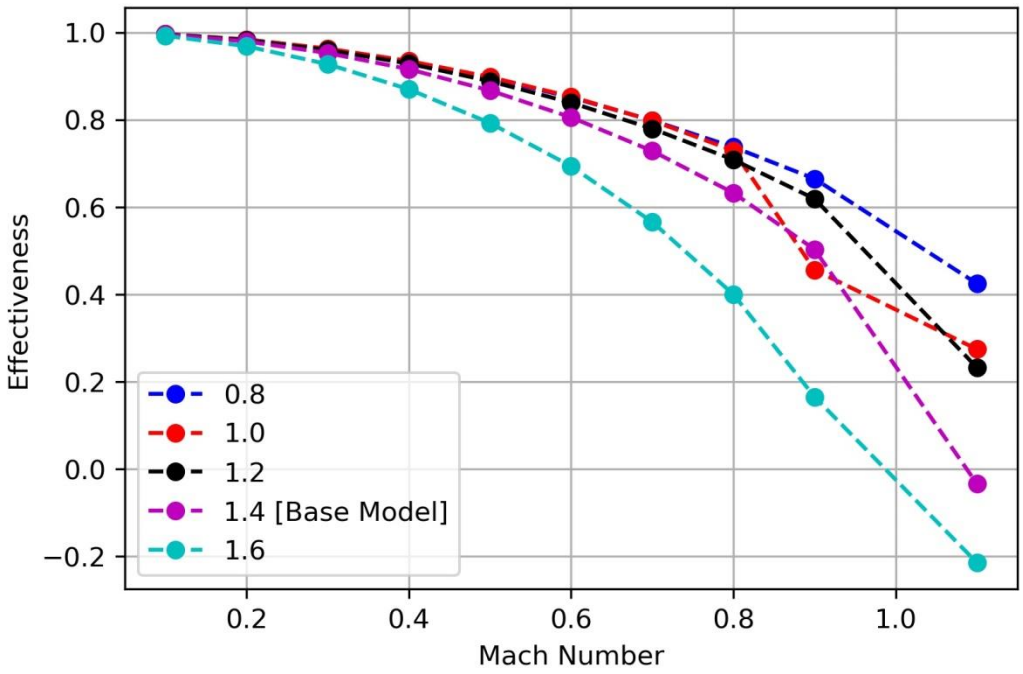

Figure 5.21. Aspect Ratio Effect on Vertical Tail Yaw Effectiveness

5.3.6 Effects of Taper Ratio

The taper ratio (λ) is determined by calculating the ratio of the tip chord (C_t) to the root chord (C_r), as described in Equation 5.6:

$$\lambda = \frac{C_t}{C_r} \tag{5.6}$$

Reducing the taper ratio leads to a stiffer vertical tail structure. The taper ratio of the vertical tail can be adjusted by modifying the length of the tip chord while keeping the span length and root chord length constant. According to Raymer in "Aircraft Design" [36], the typical taper ratio for a fighter vertical tail ranges from 0.2 to 0.4. In this study, the base model has a taper ratio of approximately 0.33. In order to examine the influence of the taper ratio, the yaw effectiveness of the vertical tail was evaluated at sea level for various configurations: 0.20, 0.25, 0.33, 0.35, and 0.40. Figure 5.22 illustrates visual representations of the analyzed vertical tail configurations. In order to assess the impact of the taper ratio change, modifications were made to the vertical tail aerodynamic model to reflect the planforms shown in Figure 5.22. Specifically, when decreasing the taper ratio, updates were applied to the aerodynamic mesh associated with the vertical tail. Furthermore, adjustments were made to the structural model, resulting in a tighter vertical tail configuration while maintaining the component's weight. These structural refinements included repositioning the beam elements, contributing to developing an inherently stiffer vertical tail structure.

As illustrated in Figure 5.23, notable enhancements in yaw effectiveness were observed across all speeds, effectively resolving the issue of rudder reversal. Notably, minimal variations in yaw effectiveness values were observed within the low dynamic pressure speed range within the low-speeds. The influence of a shorter distance between the center of pressure and the elastic axis, coupled with the inherent strength of the vertical tail, becomes increasingly apparent as dynamic pressure increases. These observations highlight the impact of taper ratio changes on yaw effectiveness values.

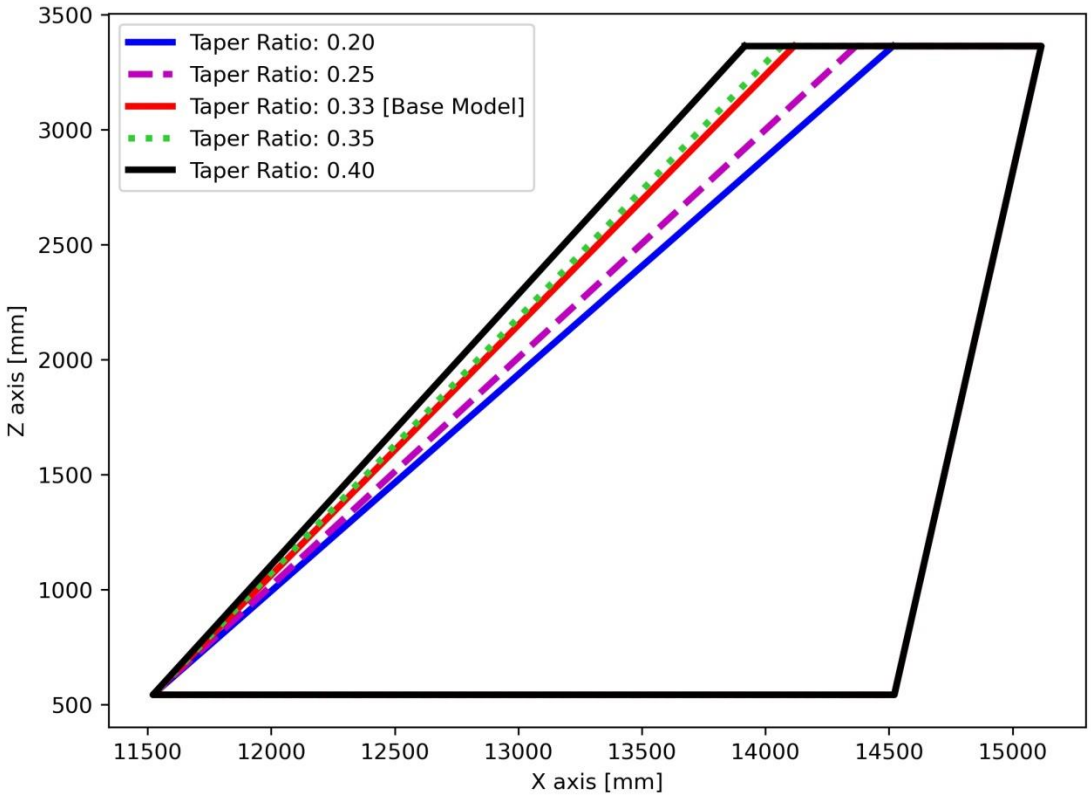

Figure 5.22. Alternative Planforms for Investigation of Taper Ratio Effect

As the taper ratio decreases, the vertical tail becomes stiffer, leading to increased effectiveness values. For instance, at the highest taper ratio of 0.40, the effectiveness value drops to -11.90% in 1.1 Mach and sea level conditions. In contrast, the lowest taper ratio of 0.2 yields significantly higher effectiveness, reaching up to 11.24%, as illustrated in Figure 5.23. Notably, when the taper ratio was set to 0.25, the issue of rudder reversal was successfully resolved, and the effectiveness value continued to rise as the taper ratio further decreased.

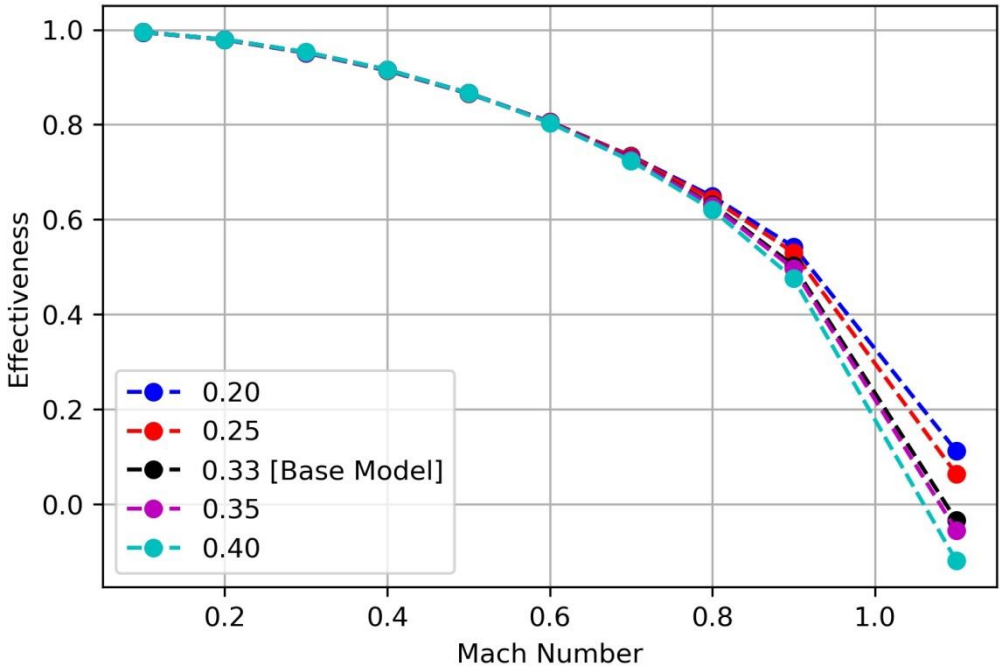

Figure 5.23. Taper Ratio Effect on Vertical Tail Yaw Effectiveness

5.3.7 Effects of Overhang Distance

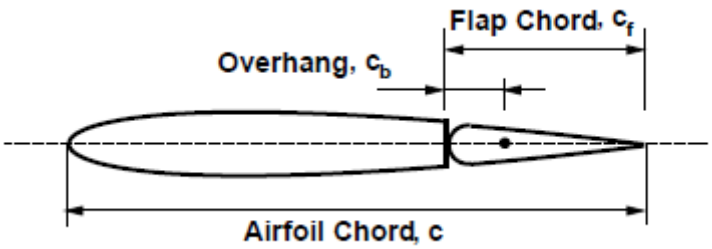

Figure 5.24. Definition of Overhang Distance [41]

The rudder overhang distance (c_b) is the offset between the hinge line location and the rudder's leading edge, as shown in Figure 5.24. Positioning the hinge line further back reduces the hinge moment generated on the rudder. A high hinge moment value is observed at the rudder hinge in the baseline configuration when no overhang distance is present for a rudder deflection of 0.1 rad and a Mach number of 0.9. Table 5.1 presents the hinge moment values corresponding to various overhang distances, expressed as a percentage ratio relative to the rudder's chord length. The results demonstrate that increasing the flap overhang leads to a decrease in the rudder hinge moment. The results imply that the hinge line should be positioned at 40% of the chord length to get the best overhang distance, as shown by the red colour as minimum value of the absolute hinge moment in Table 5.1.

Table 5.1. Rudder Hinge Moment Values vs. Hinge Line Location

Hinge Line Location [% at rudder chord length]	**Hinge Moment [N.m]**	**Absolute Value of Hinge Moment [N.m]**
0	2375	2375
10	1870	1870
20	1331	1331
30	754	754
40	137	137
45	-189	189
50	-527	527
55	-878	878
60	-1242	1242

Enhancing the rudder yaw effectiveness is closely associated with reducing the hinge moment generated on the rudder. The impact of the overhang distance on rudder yaw effectiveness is illustrated in Figure 5.25. In order to show a comparison, the hinge line was positioned at various locations relative to the rudder chord length: 0%, 10%, 20%, 30%, and 40%, respectively. These configurations were compared to the base model value. Only the location of the rotational spring

connected to the vertical tail and rudder was altered. It is assumed that no other parameters have been changed. A decrease in hinge moment yields enhanced yaw effectiveness in the subsonic region, as illustrated in Figure 5.25. However, when dynamic pressure increases within the supersonic regime, the distance between the rudder force and the vertical tail becomes more significant. In this context, the reduced hinge moment benefits are counterbalanced by the increased distance, resulting in no additional advantage for mitigating rudder reversal. However, it is worth noting that altering the hinge line position does not fix the rudder reversal because even if the force generated decreases, this effect is counterbalanced as the distance between the hinge and the elastic axis of the vertical tail increases. To summarize, shifting the hinge line towards the rear contributes to a favorable increase in effectiveness, assuming no reversal occurs. However, it does not solve the control surface reversal problem.

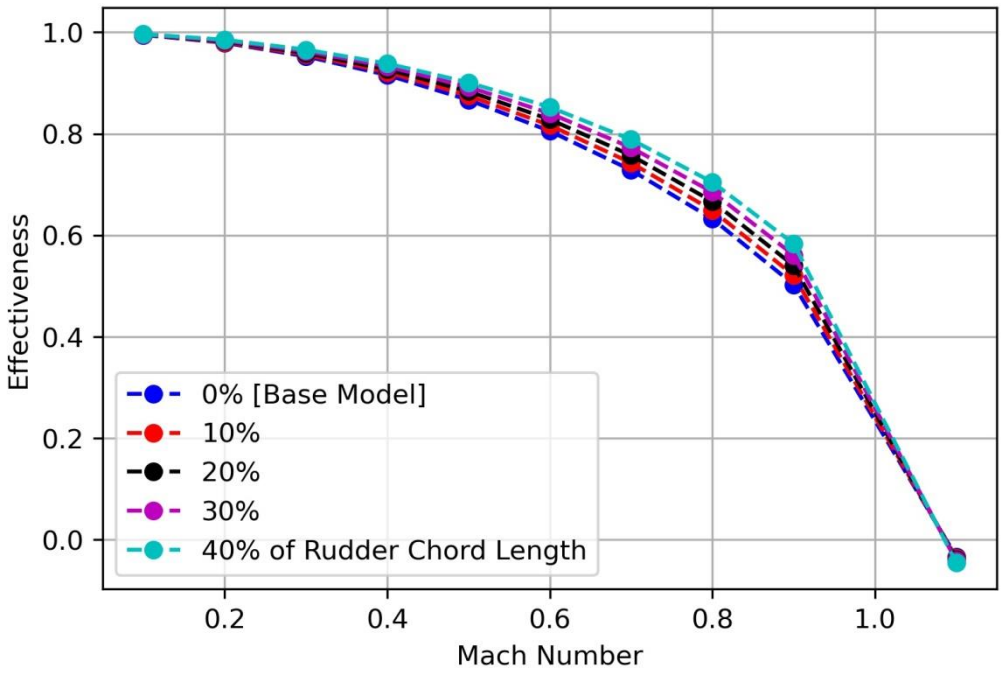

Figure 5.25. Overhang Distance Effect on Vertical Tail Yaw Effectiveness

CHAPTER 6

CONCLUSIONS

6.1 General Conclusions

The thesis aimed to comprehensively investigate the impact of various design parameters on rudder yaw effectiveness in order to address the issue of low vertical tail yaw effectiveness or rudder reversal in aircraft with twin vertical tails. These parameters included torsional stiffness, trailing edge sweep angle, rudder-vertical tail chord ratio, actuator stiffness of the rudder, aspect ratio, taper ratio, and overhang distance. By analyzing the different vertical tail configurations, the study sought to understand the influence of these design parameters on rudder yaw effectiveness. The effectiveness values obtained were calculated and visually presented to provide effective solutions for aircraft with twin vertical tails experiencing low vertical tail yaw effectiveness or rudder reversal problem.

Chapter 2 of the thesis contained a thorough literature review examining relevant studies about control surface effectiveness analysis and developing a reduced aeroelastic model. The findings and insights from these studies played a crucial role in formulating solutions for the identified issue.

Before conducting the control surface reversal analyses and obtaining effectiveness values from stability control derivative coefficients, the thesis started with the theory of static aeroelastic analyses. Chapter 3 provided an in-depth understanding of the governing equations and solution procedures implemented in the MSC.Nastran™ software.

Chapter 4 introduced the aeroelastic modeling process, consisting of three key phases. Firstly, a detailed structural model was created in order to accurately represent the aircraft's structural components and connections. Secondly, an

aerodynamic model was developed using two-dimensional panels to simulate airflow and to capture the aerodynamic forces. Finally, a spline relationship was established to transfer displacements and loads accurately between the structural and aerodynamic models. By integrating these phases, a comprehensive representation of the aircraft's aeroelastic behavior was achieved, allowing for thorough investigations of its performance under varying design parameters and operating conditions. The structural model employed as one-dimensional beam elements, while the aerodynamic model utilized the two-dimensional panels. OpenVSP and the MSC Patran FlightLoads™ (FLDS) package program were employed to generate the finite element model geometry and create the aerodynamic model mesh, respectively. Additionally, indigenous Python codes were developed to automate the rapid creation of FE models with different parameters.

Chapter 5 of the thesis focused on finding solutions for the identified control surface reversal problem. The analysis specifically looked at the issue at sea level altitude. Different design modifications were examined by conducting a series of evaluations, such as changes in torsional stiffness, trailing edge sweep angle, rudder-vertical tail chord ratio, rudder-vertical tail chord ratio, actuator stiffness of the rudder, aspect ratio, taper ratio, and overhang distance. The goal was to understand how these modifications affected the control surface reversal and explore potential solutions. The systematic assessment of these parameters provided insights and potential resolutions to address the identified problem.

In summary, in the thesis study four fundamental maneuvers' effectiveness values were computed throughout the flight envelope. The primary concern requiring improvement for an aircraft having a twin vertical tail was yaw effectiveness. Also, increasing the overhang distance and actuator stiffness cannot solve the rudder reversal problem, if there is any. However, they can improve the effectiveness value if no reversal issue exists. On the other hand, increasing the torsional stiffness, rudder-vertical tail chord ratio, and decreasing the aspect ratio, taper ratio, and trailing edge sweep angle proved effective in resolving the rudder reversal

problem and enhancing the overall rudder yaw effectiveness in the supersonic region.

6.2 Recommendations for Future Work

This study included static aeroelastic analyses in determining the effects of the seven design parameters mentioned above on the rudder yaw effectiveness. The study may be extended for the other design parameters such as rudder structural strength, vertical tail position, cant angle of the vertical tail, vertical tail incidence, etc.

MSC.Nastran™ uses the Doublet Lattice Method (DLM) for aeroelastic analysis in aircraft design for subsonic and supersonic regimes. However, this method has limitations in handling the transonic regime and phenomena like shock waves. Computational Fluid Dynamics (CFD) solvers based on higher-fidelity methods, such as the Euler/Navier-Stokes equations, are necessary to enhance accuracy and correct pressure coefficient values in the transonic region as a further improvement.

REFERENCES

[1] NATO RTO Meeting Proceedings (2000) "Structural Aspects of Flexible Aircraft Control, " North Atlantic Treaty Organization/Science and Technology Organization Rept. RTO-MP-36.

[2] Bueno, D. D., & Dowell, E. H. (2020). Revisiting the Fundamentals of Control Surface Reversal Including Nonlinear Effects. Journal of Aircraft, 57, 1212–1219. doi:10.2514/1.C035885

[3] Kolonay, R. M. (2001). Computational Aeroelasticity - METU | Aerospace Engineering. Available: http://www.ae.metu.edu.tr/~yyaman/avt086/Kolonay/Ray_Kolonay_6.pdf. (Accessed: Jan 11, 2022).

[4] Schweiger, J., Weiss, F., & Kullrich, T. (2000). Active aeroelastic design of a vertical tail for a fighter aircraft. 8th Symposium on Multidisciplinary Analysis and Optimization. Published. https://doi.org/10.2514/6.2000-4828

[5] Glenn Research Center. (2023). Vertical Tail - Rudder. NASA. Available: https://www.grc.nasa.gov/www/k-12/VirtualAero/BottleRocket/airplane/rud.html

[6] "Boeing: FA-18-Super-Hornet" Available: https://www.boeing.com/defense/fa-18-super-hornet/#/gallery. (Accessed: Feb 05, 2023).

[7] Collar, A. R. (1946). The Expanding Domain of Aeroelasticity. *The Journal of the Royal Aeronautical Society, 50*(428), 613-636. doi:10.1017/s0368393100120358

[8] Bisplinghoff, R. L., & Ashley, H. (1955). *Principles of Aeroelasticity*. N.Y: Dover Publications.

[9] Hodges, D. H., & Pierce, G. A. (2011). *Introduction to Structural Dynamics and Aeroelasticity*. Cambridge: Cambridge University Press.

[10] "Aeroelasticity in Turbomachines." EPFL, Available: https://archiveweb.epfl.ch/gtt.epfl.ch/index.html%3Fp=233.html (Accessed: Feb 05, 2023).

[11] Pugsley, A. (1937). Control Surface and Wing Stability Problems. The Aeronautical Journal, 41(323), 975-996. doi:10.1017/S0368393100110971

[12] Broadbent, E. G., & Mansfield, O. (1947). Aileron Reversal and Wing Divergence of Swept Wings.

[13] Molyneux, W. G., & Broadbent, E. G. (1950). Determination of Reversal Speed of a Wing with a Partial-Span Flap and Inset Aileron.

[14] Goland, L. (1952). Aileron Reversal Research of Straight and Swept Wings at High Subsonic Speeds. Cornell Aeronautical Lab Inc Buffalo NY.

[15] Hedgepeth, J. M., & Kell, R. J. (1954). Rolling Effectiveness and Aileron Reversal of Rectangular Wings at Supersonic Speeds.

[16] Horton, W. H. (1943). Critical Reversal Speed. Aircraft Engineering and Aerospace Technology, 15, 319–324. doi:10.1108/eb031070

[17] Pearson, H. A., & Aiken, W. S. (1944). Charts For The Determination Of Wing Torsional Stiffness Required For Specified Rolling Characteristics or Aileron Reversal Speed.

[18] Fischel, J., Naeseth, R. L., Hagerman, J. R., & O'hare, W. M. (1952). Effect of aspect ratio on the low-speed lateral control characteristics of untapered low-aspect-ratio wings equipped with flap and with retractable ailerons (No. NACA-TR-1091).

[19] Andersen, G., Kolonay, R., & Eastep, F. (1998). Control-surface reversal in the transonic regime. Journal of Aircraft, 35, 688–694. doi:10.2514/2.2378

[20] Andersen, G., Forster, E., Kolonay, R., & Eastep, F. (1997). Multiple control surface utilization in active aeroelastic wing technology. Journal of aircraft, 34(4), 552-557.

[21] Ricketts, R. H. (1983). Structural Testing For Static Failure, Flutter And Other Scary Things.

[22] Mantegazza, P., & Ricci, S. (1990). Direct approach to the analysis of control reversal and its sensitivity. AIAA Journal, 28, 1995–1996. doi:10.2514/3.10510

[23] Pendleton, E. W., Bessette, D., Field, P. B., Miller, G. D., & Griffin, K. E. (2000). Active aeroelastic wing flight research program: technical program and model analytical development. Journal of Aircraft, 37, 554–561. doi:10.2514/2.2654

[24] Yoon, N. K., Chung, C. H., Na, Y. H., & Shin, S. J. (2012). Control reversal and torsional divergence analysis for a high-aspect-ratio wing. Journal of Mechanical Science and Technology, 26, 3921–3931. doi:10.1007/s12206-012-0889-2

[25] Rose, J. B. R., & Jinu, G. R. (2015). Influence of aeroelastic control reversal problem in the airplane lateral stability modes. Proceedings of the Institution of Mechanical Engineers, Part G: Journal of Aerospace Engineering, 229(3), 517-533.

[26] Qiu, J., & Ang, H. (2019). Improving aileron effectiveness based on changing the position of aileron connectors. International Journal of Aerospace Engineering, 2019. doi:10.1155/2019/5046395

[27] Javed, Y., & Khan, N. S. (2019). Estimation of Rolling Effectiveness and Control Reversal for Aeroelasticity Effects. In 2019 16th International Bhurban Conference on Applied Sciences and Technology (IBCAST) (pp. 106-112). IEEE.

[28] Nicolosi, F., Ciliberti, D., Vecchia, P. D., Corcione, S., & Cusati, V. (2017). A comprehensive review of vertical tail design. Aircraft Engineering and Aerospace Technology, 89, 547–557. doi:10.1108/AEAT-11-2016-0213

[29] Singh, A. K., & Nichols, C. W. (1988). Derivation of an equivalent beam model from a structural finite element model. In Proceedings of the MSC 1988 World Users Conference.

[30] Elsayed, M. S. A., Sedaghati, R., & Abdo, M. (2009). Accurate stick model development for static analysis of complex aircraft wing-box structures. AIAA Journal, 47, 2063–2075. doi:10.2514/1.38447

[31] Nazar, N., Gandhi, P. A., Rajendran, S., & George, M. (2020). Control effectiveness of wing with elevon of a typical reusable launch vehicle. *Lecture Notes in Civil Engineering*, 213–224. doi:10.1007/978-3-030-55115-5_21

[32] Ashley, H., Rock, S. M., Digumarthi, R., Chaney, K., & Eggers Jr, A. J. (1994). Active Control for Fin Buffet Alleviation. United States Air Force Research Laboratory Report WL-TR-93-3099.

[33] Rodden, W. P., & Johnson, E. H. (1994). MSC/NASTRAN Aeroelastic Analysis User's Manual. Version, 68, 237-257.

[34] OpenVSP - VSP Hangar. (2022). Available: https://openvsp.org/ (Accessed: Jan 11, 2022).

[35] Roskam, J. (2005). *Airplane Design Part I: Preliminary Sizing of Airplanes*. DARcorporation.

[36] Natella, M., & De Breuker, R. (2019). The effects of a full-aircraft aerodynamic model on the design of a tailored composite wing. *CEAS Aeronautical Journal*, *10*(4), 995–1014. https://doi.org/10.1007/s13272-019-00366-5

[37] ZAERO v.9.3 User's Manual. (2019). Available: https://zonatech.com/Documentation/ZAERO_9.3_Users_Full_Electronic.pdf

[38] Hayes, William Brian and Kelan D. Sisk. (2008). "Prevention of External Store Limit Cycle Oscillations on the F/A-18E/F Super Hornet and EA-18G Growler Aircraft."

[39] Gudmundsson, S. (2014). The Anatomy of the Wing. General Aviation Aircraft Design, 299–399. https://doi.org/10.1016/b978-0-12-397308-5.00009-x

[40] Raymer, D. (2012). Aircraft Design: A Conceptual Approach. American Institute of Aeronautics and Astronautics, Inc..

[41] Shen, J., Yang, M., & Chopra, I. (2006). Swashplateless Helicopter Rotor System With Trailing-Edge Flaps For Flight And Vibration Controls. Journal of Aircraft, 43(2), 346-352.

[42] Yurtsever, A., & Yaman, Y. (2022). 9. ULUSAL HAVACILIK VE UZAY KONFERANSI. Çift Dikey Kuyruklu Bir Uçağın Kanatçık Tersliğinin ve Dümen Etkinliğinin İncelenmesi. İzmir. Available: http://uhuk.org.tr/bildiri.php?No=UHUK-2022-103.

APPENDICES

A. GUI of Structural Model Generator

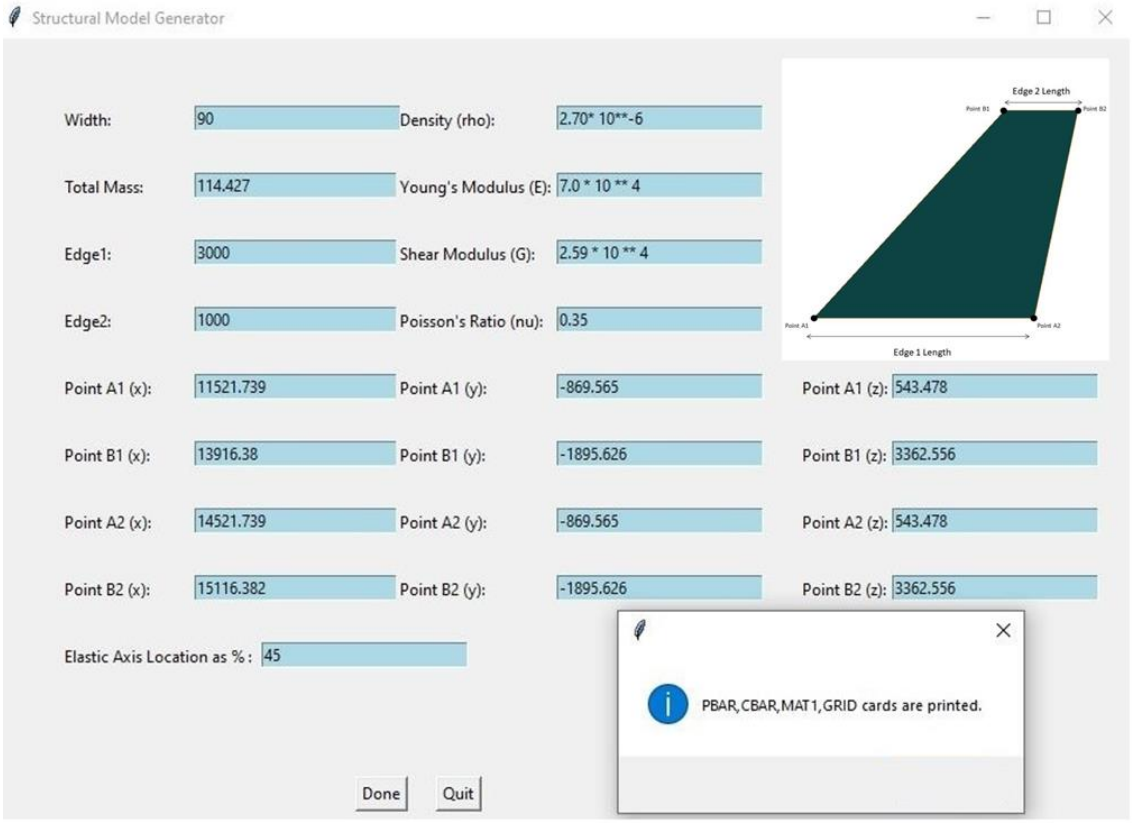

Figure A.1 GUI of Structural Model Generator

The GUI aims to create a structural finite element model using one-dimensional (1D) beam elements. The Python code for this purpose incorporates various procedures to establish the structural model based on user inputs. Figure A.1. gives the values used as an example while creating the vertical tail.

Here is a detailed breakdown of the GUI and code work, as shown in Figure 4.2. :

- The input for the structural model includes the start and end coordinates of aircraft components such as the fuselage, wing, horizontal tail, vertical tail, and control surfaces. The beam-stick structural model location changes with respect to taken the input of elastic axis location.

- Linear interpolation is used to determine the positions of nodes for creating beam elements.

- The sectional lengths of the beam elements need to be specified. This calculation is interpolated from given Edge 1 and Edge 2 lengths. These lengths are obtained by measuring relevant dimensions from the outer geometry of the components. The lift and control surfaces require corresponding chord lengths.

- The mesh convergence study determines the number of beam elements constituting each component. The node positions for these elements are calculated using the start and end points of the components and the assigned number of elements.

- The weight distribution of each component is allocated proportionally to the beam elements, considering the square of the provided sectional lengths. This ensures that the mass is distributed accurately along the structure.

- The required cross-sectional area for each beam element is computed using the input data on material density to achieve the desired mass.

- The second area moments of inertia for the beam elements are calculated based on their sectional lengths.

- The resulting values, including the node positions and calculated parameters, are formatted according to the requirements of the MSC.Nastran™ program. This involves creating cards such as PBAR, CBAR, GRID, and MAT1, which define the structural properties of the beam elements.

B. GUI of Aerodynamics Model Generator

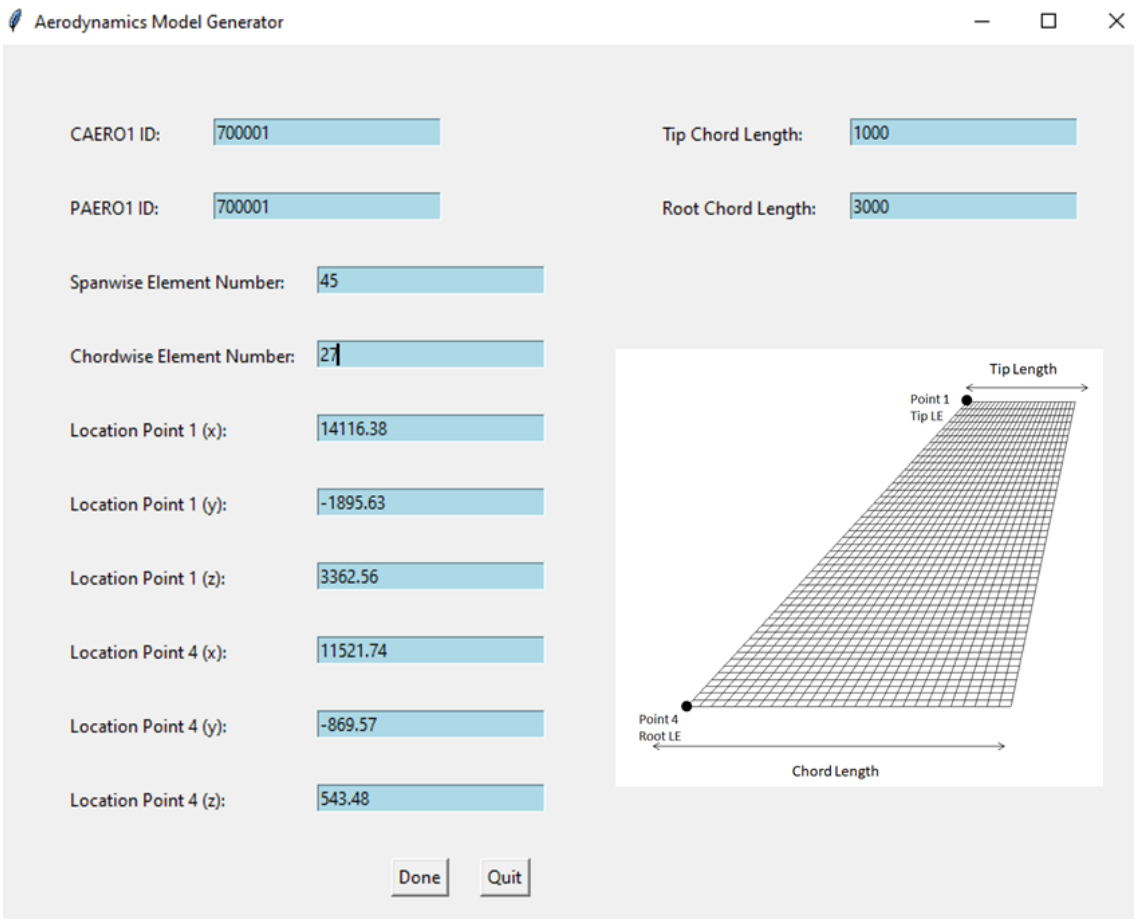

Figure B.1 GUI of Aerodynamics Model Generator

The Aerodynamic Model Generator GUI makes it easier to model how changes in design parameters affect the aerodynamic mesh and simulation results. This tool simplifies the aerodynamics modeling process for aeroelasticity analysis by updating the mesh according to modified parameters. As an example, Figure B.1 provides the values used when creating the vertical tail.

The code generates aerodynamic model cards based on user inputs obtained from a GUI. This GUI enables users to quickly apply design changes to the model, including modifications to design parameters found in Appendix C. By utilizing this aerodynamics model generator GUI, users can easily make changes to the

model based on identified design parameter variations. The code takes inputs such as point coordinates, element IDs, and spanwise and chordwise element numbers to construct the CAERO1 and PAERO1 cards. Additionally, users input span length and chord length as parameters. The code writes the constructed cards to a BDF file, incorporating the user-provided inputs.

C. GUI of Design Parameter Changer

Figure C.1 GUI of Design Parameter Changer

Appendix C provides information on the Python codes developed for each design parameter. Specific codes were created for each parameter to update the corresponding design values. These updated values were then used as inputs to modify the design and complete the analyses.

The graphical user interfaces (GUIs) presented in Appendix A and Appendix B were utilized to facilitate the design updates found in Appendix C. Figure C.1 shows the GUI interfaces that takes input for the design changes.

Here's a breakdown of the how each design parameter updated:

- Torsional Stiffness: The input values modify the vertical tail beam element's polar second area moment of inertia (J) values to modify GJ values.

- Trailing-Edge Sweep Angle: It calculates the vertical tail and rudder components' new positions to update the aerodynamic and structural meshes based on the specified trailing edge sweep angle. All other design parameters assumed to stay constant.

- Rudder-Vertical Tail Chord Ratio: This parameter leads to updates in the aerodynamic and structural models of the vertical tail and rudder. It involves changes in the number of aerodynamic elements for both the vertical tail and rudder. Any newly added or deleted elements are adjusted to maintain their spline relationships. Additionally, the hinge line is shifted to adjust the new leading edge location of the rudder. Furthermore, the cross-sectional lengths of the rudder beam elements are also modified as part of these updates.

- Actuator Stiffness of Rudder: The input values update the only equivalent rotational stiffness, which represents the actuator stiffness and affects the rotation of the rudder. All other design parameters kept constant.

- Aspect Ratio: It changes the structural and aerodynamic models based on the input value, modifying the height while keeping the root and tip lengths constant for vertical tail structural and aerodynamic elements.

- Taper Ratio: This parameter modifies the structural and aerodynamic models of vertical tail component by changing the tip length while keeping the root length and height constant.

- Overhang Distance: The entered value for overhang distance updates the connection point where the control surface rotates and the location of the hinge line coordinate that enables the rotation.